

This is the post-print version of the following article:

Quintanilla, M; Liz-Marzán, LM; [Guiding Rules for Selecting a Nanothermometer](#), NanoToday, Volume 19, April 2018, Pages 126-145

DOI: [10.1016/j.nantod.2018.02.012](https://doi.org/10.1016/j.nantod.2018.02.012)

This article may be used for non-commercial purposes in accordance with Elsevier Terms and Conditions for Self-Archiving.

Guiding Rules for Selecting a Nanothermometer

Marta Quintanilla^{1*}, Luis M. Liz-Marzán^{1,2}

¹CIC BiomaGUNE and CIBER-BBN. Paseo de Miramón 182, 20014 Donostia - San Sebastián, Spain

²Ikerbasque. Basque Foundation for Science, 48013 Bilbao, Spain

*Corresponding author's e-mail: mquintanilla@cicbiomagune.es

Abstract

Temperature is a basic parameter influencing the behavior of systems in physics, chemistry and biology. From living cells to microcircuits, a wide range of cases require thermometry techniques that can be applied to reduced areas, offering sub-micrometric resolution and high accuracy. Since traditional thermometers cannot be applied in such systems, alternative tools have been specifically designed to measure temperature at the nanoscale; including scanning thermal microscopy, non-contact optical techniques or various types of luminescent nanoparticles. Each option presents interesting advantages, but also limitations that need to be considered and understood. We provide here an overview of the main currently available nanothermometry tools, discussing their pros and cons toward potential applications.

Keywords: Temperature, nanoparticles, thermal mapping, luminescence, spectroscopy

1. Introduction

The development of techniques to fabricate micrometric devices has largely expanded the number and variety of fields that are evolving towards miniaturization, as is the case of microelectronics or microfluidics. On the other hand, the reduction of the size of materials gives rise to new physical properties of matter that can also be exploited in a variety of technological applications, as is the case of the use of plasmonic and fluorescent nanoparticles in medicine or biological imaging. The access to the nanometer size range opens many new paths for research, but also brings the need to implement new techniques to characterize the prepared devices. Temperature is one of the most basic parameters influencing any physical or chemical process. However, the traditional strategies to measure temperature cannot be applied to the nanoscale, either because of size limitations regarding the thermometer or due to a limited access to the area of interest. As a consequence, nanothermometry has emerged aiming to the development of thermometers with micrometric or sub-micrometric spatial resolution.

The problem is further complicated by the fact that not only the thermometric tool needs to be adapted to the new size range, but also the theoretical background (thermodynamics or mechanical statistics) is to be modified to work at the nanometer scale. According to the zeroth law of thermodynamics, if we have three systems, A, B and C, such that A and B are in thermal equilibrium with C, then A and B must be in thermal equilibrium with each other and thus they all have the same temperature. This is how the concept of temperature arises classically, as a parameter that can be measured, and indeed is this law in itself which allows us to measure temperature; a thermometer must be in thermal equilibrium with the system to be characterized. Instead, if we look at statistical mechanics to find a definition of temperature, then we find that it is given by the variation rate of entropy with the internal energy of the system. Either way, with

these definitions in mind, there is a minimum volume of material that needs to be considered for the standard concepts of thermal equilibrium and intensity of temperature to hold [1-3].

There is thus a thermodynamic limit regarding size that defines whether the standard thermodynamic description of a system remains valid [3, 4]. With the development of nanothermometry, the discussion on the size range that applies moved from a purely academic discussion to a practical one. Accordingly, a few approaches have been proposed, as well as a validity length scale based on a one-dimensional model, i.e. a chain of atoms. This length scale depends on the specific material under discussion, through its lattice constant and Debye temperature, but it brings some general conclusions (**Figure 1**): the limiting length at low temperatures (<10 K) is rather restrictive, and can be in the order of 1 cm, but it rapidly decreases for higher temperatures and from 100 K onwards the limiting length becomes roughly constant and is close to one micrometer in the case of crystalline silicon, and slightly smaller in the case of carbon nanotubes. Even though these are approximate values linked to a simplified model, such size restrictions need to be kept in mind when nanothermometry results are discussed [3, 5, 6].

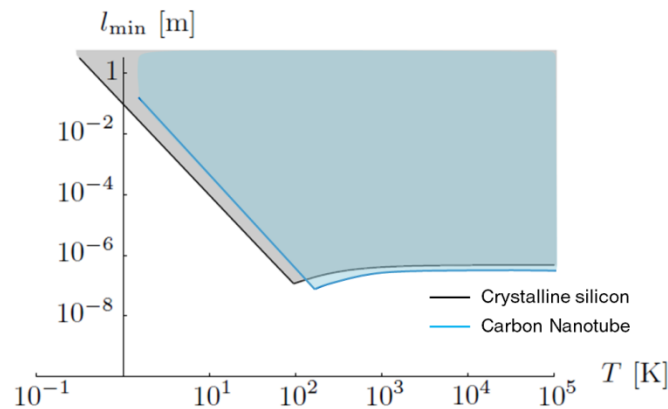


Figure 1. Minimal length scale (l_{min}) on which intensive temperatures exist in two selected materials: elongated wire of crystalline silicon (black line) and carbon nanotubes (blue line).

Local temperature exists in the shaded areas. Adapted from Ref. [3] with permission from Taylor and Francis Ltd (<http://www.tandfonline.com>).

The availability and variety of thermometry options at the nanoscale is already large, and novel methods are proposed every year [7-11]. As a consequence, it is possible to start exploiting them to get practical information on temperature, but the path is not easy and many problems may arise in doing so. An illustrative example is the open discussion related to intracellular temperature. Several nanothermometry papers have addressed the problem of the internal temperature of a living cell, which can provide information about its metabolism [12, 13]. Different techniques have been used, ranging from insertion of a micro-thermocouple in the cell [14], a glass micropipette full of luminescent thermometric material [15], or by delivering different luminescent molecules or nanoparticles in the cytoplasm or the nucleus [16-19]. These methods allow us to detect thermal differences between cells or between different areas inside the cell (nuclei, mitochondria, centrosomes and cytoplasm), ranging from 0.5 to 2.9 °C in different reports, but which are assigned to thermogenesis processes that are triggered in different ways. Meanwhile, theoretical calculations have been made on the basis of standard thermodynamic considerations and scaling laws that take into account the size of cells or their organelles, the levels of glucose that can eventually be transformed into thermal energy, and even the existence of a membrane that can affect the thermal distribution. According to these calculations the measured thermal increase should not be larger than 10^{-4} °C, a value that is clearly lower than the measured ones [20]. Controversy continued when discussing the potential sources of error related to both the experimental techniques and the theoretical calculations, but full agreement has not been reached yet [21-23].

It is clear from the above discussion, that much work is still needed to unveil the thermal behavior of chemical, physical and biological processes at the nanoscale. Fundamental

thermodynamic studies, device-performance monitoring, cell physiology studies or medical treatments; the fields of application of nanothermometry are many and diverse, and so are the requirements for nanothermometers. Indeed, there is no universal thermometer that can be used in every case, but rather different options that adapt better to each different situation. In general, a thermometer is characterized by how accurately it determines temperature and by the thermal range within which it can work. Both features are fundamentally limited by the physical laws that govern each particular thermometer design, as well as by its chemical stability. However, the instrumental set-up needed in each case also plays an important role, as it can limit the thermal accuracy through the signal-to-noise ratio and may impose restrictions on the type of samples that can be studied.

It is our intention in this manuscript to review the main nanothermometry strategies, to define their pros and cons, the range of applications where they may excel but also their limitations. **Figure 2** shows a summary of standard thermal and spatial resolutions of the techniques that will be discussed below. We briefly start with contact techniques, mainly based on scanning microscopes, continue with non-contact optical techniques and then discuss the main categories of luminescent nanoparticles for nanothermometry (orange dots in Figure 2), which can be considered as a different category of semi-contact thermometry strategies.

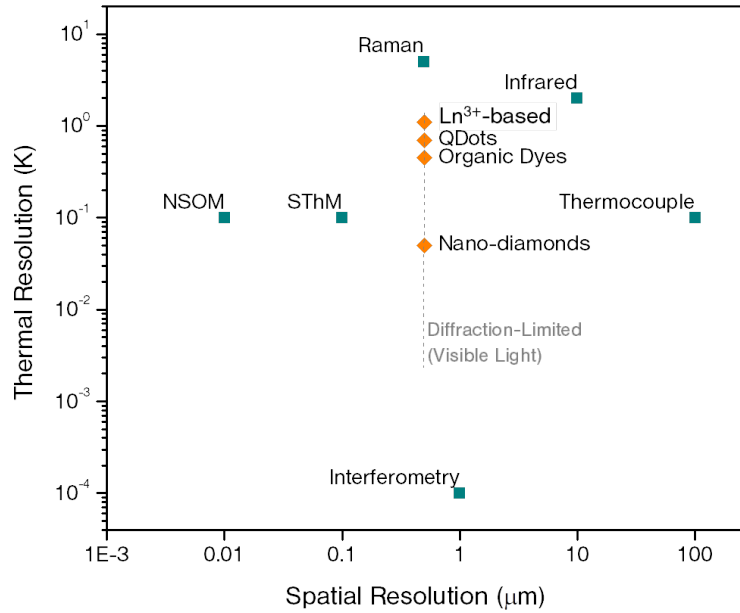


Figure 2. Typical thermal resolution vs. spatial resolution for various thermometry techniques, seeking sub-micrometric resolution. Orange dots indicate techniques based on luminescent nanoparticles. In this case, the spatial resolution is given by the experimental set-up (usually a microscope) and thus it is diffraction-limited. As a consequence, the precise spatial resolution will depend on the wavelength of the light applied, so it will be smaller for UV probes and larger for near-IR probes.

2. Some insights on the figures of merit of a thermometer

When a measuring system is proposed, its performance must be numerically stated, in such a way that it allows understanding how accurate the measured value will be. Furthermore, it should be possible to establish a fair comparison with alternative measurement systems. The most commonly reported figures of merit in nanothermometry are sensitivity and thermal resolution [10]. In all of the techniques discussed in this manuscript, temperature is measured indirectly, through changes in electrical current, light intensity, peak shifts, etc. and thus these parameters will be the indication, Q , of temperature. The sensitivity, S , gives an idea of the smallest amount

of change that temperature can provoke in the indication, and thus, it is defined as the rate of change of Q related to temperature, T:

$$S = \left| \frac{\partial Q}{\partial T} \right| \quad (1)$$

In order to facilitate comparison between systems based on different indications, the sensitivity is often normalized to the value of Q, giving rise to the relative sensitivity:

$$S_R = \left| \frac{1}{Q} \frac{\partial Q}{\partial T} \right| \quad (2)$$

Sensitivity is thus expressed in units of indication divided by K (or equivalently, °C) while relative sensitivity is measured in units of K⁻¹ (or °C⁻¹), allowing comparison, but it can also be found as a percentage of change (%K⁻¹) obtained by multiplying its value by 100.

According to the definition, the sensitivity of a thermometer is linked to the physical mechanism that triggers a change in the indication, and may also depend on the materials chosen to construct the thermal probe. However, the precision of an actual measurement will also depend on specific details related to how the measurement is performed. For instance, for a thermometer based on light intensity, the uncertainty of the measurement is linked to the signal-to-noise ratio in the spectrum; if the signal is weak and the recorded spectrum is noisy the result cannot be highly precise. In this case, precision will depend on the excitation power, how it is focused on the sample, the specific detector, etc. It should be noted that a precise result is not necessarily giving the exact real temperature (this would be an accurate result). Instead, it is a result with a small uncertainty. Precision is thus closely linked to the thermal uncertainty of the measurement (ΔT), which is an estimate of the dispersion of values within which the true temperature value is expected to lie [10]. Following the standard formula for the propagation of error, if Q only

depends on temperature, its uncertainty will be given by $\Delta T = |\partial T / \partial Q| \Delta Q$. Then, precision is a normalized version, defined by $(\Delta T / T) \times 100$, and it is given as a percentage.

In order to give a numerical value to the precision, the above definitions imply that a ΔQ is needed. More often, ΔQ is calculated from the standard deviation (σ) of reproducibility and/or repeatability experiments. Repeatability experiments are carried out by determining the indication over a short period of time, always at the same location, using the same system that is controlled by the same operator and under the same conditions. Instead, reproducibility involves taking measurements at different locations and using different systems, controlled by different operators. For a detailed description of the ways in which repeatability (and reproducibility) can be calculated, the reader is directed to excellent specialized reviews [24, 25]. Besides precision, determining whether a thermometric system can also yield accurate values requires the use of a standard, in this case a sample at a known temperature, and to check whether this known value is actually measured by the system.

Thermal resolution, ΔT_{\min} , is defined to combine sensitivity (linked to the physical mechanism producing the indication) with uncertainty (connected also to the measurement procedure):

$$\Delta T_{\min} = \frac{\Delta Q}{S} \quad (3)$$

Accordingly, thermal resolution is the smallest change in temperature that causes a perceptible change in the indication, and it is measured in K [10]. When comparing values of thermal resolution corresponding to different thermal probes, it must be noted that if the standard deviation comes from repeatability measurements and not from reproducibility measurements, as is often the case, the value will be strongly dependent on the experimental set-up, including the quality of the detectors, integration time, excitation power, etc. For this reason, comparison is not

always straightforward, and it must be always done bearing in mind how measurements are performed.

3. Contact techniques

Given the many fields in which thermal information at the micrometer scale is relevant, a wide variety of strategies have been proposed to obtain it. Most of them can be classified into three main categories: electrical, mechanical and optical [7]. Following the working scheme of traditional thermocouples and thermistors, electrical techniques use a conductive probe based on the junction of two different metals, and monitor variations induced by temperature on their resistance, voltage, conductivity or electrical capacity. This can be done on the tip of a scanning probe microscope (**Figure 3**), giving rise to Scanning Thermal Microscopy [26, 27], or as a layered device through nanolithography [14]. Instead, mechanical techniques use a bi-material probe with two well differentiated thermal expansion coefficients and calculate temperature from the material bending, which can also be implemented in microscopy imaging techniques when adapted to an AFM cantilever [28]. These techniques are outstanding from the spatial resolution point of view as they keep, in principle, the characteristics of AFM-based techniques. They are convenient to study heat flow on surfaces, and have been applied to characterize microelectronic and optoelectronic devices [29] as well as some nanomaterials [30]. It is however a complex technique regarding both the experimental set-up and data analysis; at least if quantitative measurements are required, since careful considerations on heat transfer at the nanoscale between the tip and the sample should be made [27]. Their main limitation is related to the thermal reading being strictly related to the surface, thus requiring physical access to the area of study. The only exception may be the case of micro-thermocouples prepared from layers of different metals to exploit Seebeck effect for thermometry. Indeed, a tip as narrow as few

hundred nanometers made of tungsten and platinum has been used to measure intracellular temperature, obtaining a thermal resolution below 0.1 °C. However, further miniaturization of the system would involve deviations on the thermal reading [14]. Very recently, micro-thermocouples were added to the surface of sub-millimeter cell culture wells to measure the temperature variations produced due to the presence of living cells. This, together with a highly stable cell incubator, constitutes a device capable of measuring thermal changes with 10 mK uncertainty. This device is expected to shed light on the open discussion related to the maximum thermal gradient that can be established inside living cells (see further details in the introduction). The initial experiments demonstrated temperature monitoring for more than two days in different wells, and detection of thermal fluctuations due to the presence of human cancer liver cells of around 60 mK. This constitutes an interesting approach that may end up solving the issue; however, as the authors pointed out, improved spatial resolution is required to reach a clearer conclusion [31].

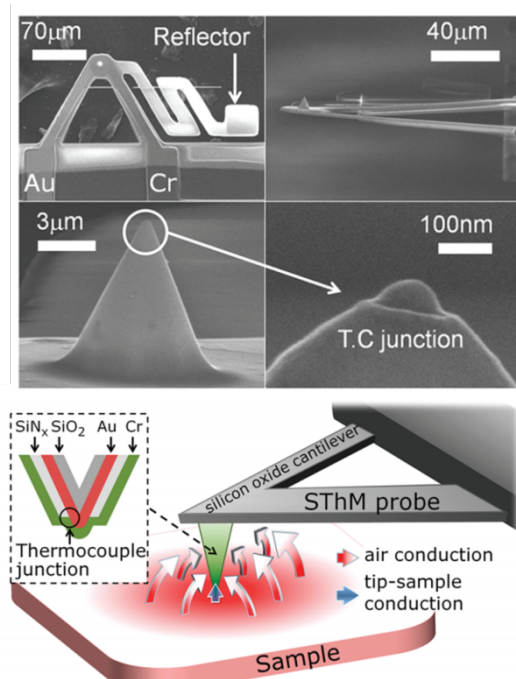


Figure 3. Scanning electrical micrographs of a cantilever adapted for thermal measurements. As shown in the scheme, the thermocouple (TC) junction where Seebeck effect takes place is located on a reduced area of the tip. The measurement is affected not only by the tip-sample conduction, but also by the conduction of air around it. Adapted with permission from Ref [26]. Copyright 2011, American Chemical Society.

An alternative mechanical strategy, which also finds inspiration in traditional ways of measuring temperature, comprises nanothermometers based on a liquid confined in a tube that contracts or dilates as a result of temperature changes. The first nanoscopic version was based on a carbon nanotube filled with gallium, and the level of the liquid inside the tube was monitored through SEM [32]. Different materials have been proposed for both the tube and the filling, but the technique has not been applied in practice [6].

All of the techniques mentioned so far can be used to determine local temperature with sub-micrometer spatial resolution but, with the exception of micro-thermocouples, they can only be applied to surfaces and require complex experimental set-ups (often a scanning microscope), thereby restricting the type of samples that can be studied. Optical methods instead can be used in a remote mode and often allow extracting information from inside the sample, not only from its surface, which is particularly relevant in biomedical applications where even in the simplest situation the object under study is not at the surface but immersed in an aqueous medium (*in vitro* studies) or is part of a living being (*in vivo* studies).

4. Non-contact techniques: exploiting light

Following the idea of bringing to the nanoscale techniques that are available at the macroscale, the first optical strategy one would think of is infrared thermal microscopy, which follows the same principle of standard infrared thermal cameras. In this case, the thermal measurement is based on the fact that every object radiates an electromagnetic field with features that depend on

its temperature. The wavelength is typically in the IR (between 2 and 12 μm), and its spectral distribution can be approximated using the theory of black-body radiation, which is used to translate the optical signal into a thermal map. In principle, this technique can be adapted to microscopy by using the same type of sensors currently used in thermal cameras, provided that the optics are tuned to the wavelengths of interest. This involves changing the design and material of all lenses, to become transparent in the mid- and far-IR ranges (typically requiring germanium-based optics). The spatial resolution is then fundamentally limited by diffraction, which for IR microscopy is within a few micrometers. Infrared thermal microscopy is a fast technique that allows two-dimensional mapping, and thus useful as contactless tool e.g. in microelectronics. However, it suffers from the same limitations as standard infrared thermal imaging, i.e. it only provides information from the surface of the sample and, since most objects are not perfect black-bodies, absolute temperatures can only be measured by considering the emissivity of each material in the area of interest, resulting in accuracies above 1 $^{\circ}\text{C}$.

Two related techniques with improved spatial resolution and 3D mapping are interferometry and Raman spectroscopy. In a simple interferometer, two different light beams (often one single beam split in two) are used. One beam passes through the sample, whereas the second one bypasses it. When both output beams are compared (by subtraction), their differences carry information about the sample. Regarding thermal imaging, interferometry has been applied to monitor changes in the refractive index of a fluid, triggered by temperature. The technique uses an even illumination source (Köhler illumination) and a wavefront analyzer, so that mapping becomes possible [33]. The performance of interferometry has been demonstrated by measuring the heat dissipated by a gold microwire, as well as bubble formation from plasmonic

nanostructures in water [34, 35]. Interferometry is a simple and fast technique to study samples immersed in fluids, only limited by the need of a model to define the refractive index of the fluid.

Raman spectroscopy can in principle be applied to a much wider spectrum of samples and experimental conditions, but it normally requires long integration times to record the optical signal, which is typically weak. The basic phenomenon behind Raman spectroscopy is called Raman scattering. When light of a certain wavelength illuminates a molecule, most of it is elastically scattered, changing the propagation direction but keeping the same wavelength (Rayleigh scattering). However, a small part of the illumination interacts with the molecule in such a way that it either absorbs or emits a small fraction of energy, and thus the wavelength of the resulting scattered light is slightly shifted (Raman scattering). The amount of energy that the molecule absorbs or emits is quantized and related to molecular vibrational modes (phonons) which are revealed through the shift of Raman scattered light. Every substance has thus a specific Raman spectrum, as vibrational modes are characteristic of each substance. Since phonons can be created or absorbed, there will be a set of peaks with higher energy than the excitation light and a second set with lower energy, both related to vibrational modes. The higher energy spectrum is known as anti-Stokes, and the lower energy one as Stokes, typically with a higher intensity. Since vibrational modes are intrinsically linked to the position of atoms in a crystal (or molecule) and to their energy, they readily reflect temperature changes that can be determined by Raman scattering. Thermal Raman imaging involves illuminating the sample with a laser, recording the scattered signal with a high-resolution spectrometer, and then analyzing the main vibrational modes in terms of peak wavelength, width or intensity to determine temperature [36]. Alternatively, temperature can be obtained from the ratio between the Stokes, I_S , and anti-

Stokes, I_{AS} , intensities of a selected Raman mode, as they are fundamentally connected following a Boltzmann distribution:

$$\frac{I_{AS}}{I_S} = \frac{(\omega_l + \omega_v)^4}{(\omega_l - \omega_v)^4} \exp\left(-\frac{\hbar\omega_v}{k_B T}\right) \quad (4)$$

where k_B is Boltzmann's constant, T is temperature, \hbar is Planck's constant, ω_v is the mode vibrational frequency and ω_l is the laser frequency [37].

As main advantages, this technique does not require a complex sample preparation, needs small volumes of material and can be applied in a wide range of environments, even during chemical reactions or under extreme conditions of pressure and temperature. Raman spectroscopy works within a wide thermal range, but it is limited at high temperatures due to a black-body radiation background (above ~ 1000 K) and at low temperatures due to the weak population of vibrational modes, mainly affecting the anti-Stokes signal. This lower thermal limit depends on experimental aspects and on the phonon frequency. Aiming to offer some guiding values, McGrane et al. estimated the applicability of equation (4) in thermometry and concluded that phonon modes $< 500 \text{ cm}^{-1}$ are needed to measure temperatures around 100 K, while to measure a temperature around 10 K a phonon mode $< 50 \text{ cm}^{-1}$ is required [37].

This technique has been used to obtain images of micro-heating devices (to determine heat transport in wires or thermal strains), to study the thermal behavior of nanomaterials such as nanotubes or graphene (**Figure 4**), and to analyze the heating efficiency of gold nanodisks [38-40]. In principle, every material is potentially a thermal probe from the Raman point of view, and thus the technique should be applicable in many different situations. However, limitations arise related to the need for transparency of the sample and by the intrinsically weak intensities of Raman signals. This could be partially solved by using long integration times or high excitation

power, but still many samples contain fluorescent species whose emission may obscure the Raman signal. Trying to overcome these limitations, nanoparticles of some materials with known Raman spectra and demonstrated thermal sensitivity have been proposed as probes for Raman thermal imaging [41]. It is however difficult to quantify the thermal and spatial resolutions, since they largely vary for each experiment, but typical thermal resolutions range between 1 and 10 °C and spatial resolution can go down to hundreds of nanometers [7, 8].

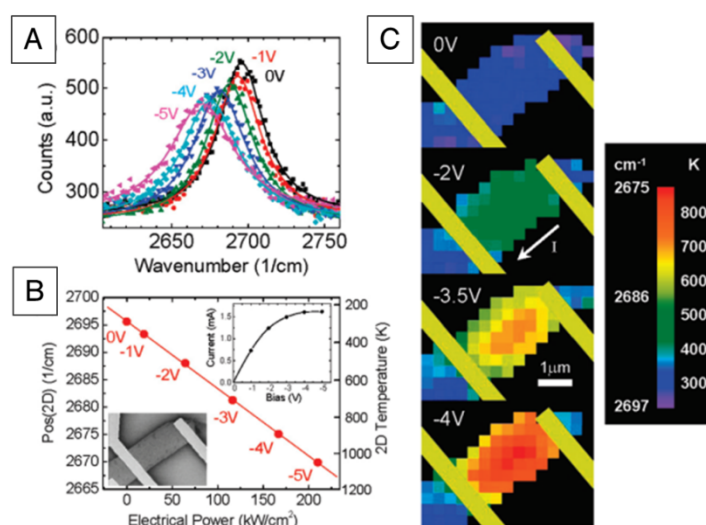


Figure 4. Example of the use of Raman spectroscopy to measure the temperature of a graphene transistor. (A) The phonon mode of graphene is shifted as a result of the applied voltage. (B) The dependence of the shift is proportional to the dissipated electric power, suggesting that Joule heating is responsible for phonon mode variations. Using a calibration step the Raman map can be translated into a 2D thermal map of the device (C). The yellow stripes represent electrical contacts on the graphene flake, as shown in the SEM inset of (B). Adapted with permission from Ref. [38]. Copyright 2009, American Chemical Society.

Infrared thermography, interferometric techniques and Raman spectroscopy can be, depending on the requirements of the experiment, successful strategies to measure local temperature in microstructured samples. However, their limitations prevented them to be implemented in biological and medical applications, two fields that can largely benefit from nanothermometry.

Temperature affects biochemical reactions inside cells, so cellular functions are strongly linked to it. Intracellular temperature can actually be used as an indicator of cellular activity. Furthermore, a local temperature increase in the cellular environment is the basis of hyperthermia therapies, which again would benefit from thermometry for an optimal application of the treatment. In terms of measuring temperature, biological environments present two main difficulties: first, samples are highly inhomogeneous regarding composition, refractive index and sometimes pH; second, the techniques should offer 3D spatial resolution, as even in the simplest case of cells cultured on a 2D layer, samples are embedded in a complex medium. Recent advances toward resolving this need are based on luminescent nanoparticles that show temperature dependent luminescence. This can be considered as a semi-contact temperature measurement, meaning that remote-sensing is obtained by excitation and emitted light traveling through the sample, but with the requirement that the nanomaterial must be located in the illuminated area. This however raises additional concerns regarding toxicity and cell internalization, so the chemical aspects of the thermometer design become particularly relevant.

The challenge of devising and synthesizing optical probes for thermometry has been resolved through a wide range of options based on very different materials. Again, each option accounts for several pros and cons that render it particularly suitable for specific situations. For example, thermometers designed for *in vitro* applications (physiology studies) and for diagnosis *in vivo* require a small range of working temperatures (30 – 40 °C) but the thermal resolution should be high (0.1 °C or higher) because temperature changes are expected to be small. Instead, alternative *in vivo* applications such as controlled photothermal therapy or thermal ablation, the working range must reach higher temperatures (60 – 70 °C), but a thermal resolution around 1 °C is

generally sufficient. We discuss below the main types of materials for nanothermometry based on luminescence, classifying them according to their composition.

5. Thermometry based on luminescent nanoparticles

5.1. Organic dyes, polymers and proteins

When considering biological applications, the most common fluorophores are probably organic dyes, which are frequently used as fluorescent markers to tag different cell components or to distinguish cells with different metabolic activity. Organic dyes are excellent markers because many of them feature high quantum yields and are thus easy to detect. However, they also present limited photostability, thus compromising the time that experiments can last and the light irradiation doses that can be applied. The same characteristics hold when organic dyes are used as thermal probes, except that now a third parameter should be considered: thermal sensitivity. The list of organic dyes with thermometric capability is long, and many are commercially available so they can be selected to specifically target the needs of a certain experiment, at least regarding emission/excitation wavelengths (mainly in the UV and visible range, but dyes with near-IR emission can also be found) or solubility [8].

The optical properties of organic dyes are determined by allowed electronic transitions. Two main types of photoluminescence can be distinguished in molecular fluorophores, depending on the spin of the excited electron: phosphorescence and fluorescence. Phosphorescence is the emission related to relaxation of a triplet state (spin parallel to that in the lower level), whereas fluorescence is emission related to relaxation of a singlet state (spin anti-parallel to that of the lower level) (**Figure 5**) [42]. Phosphorescence accounts for longer lifetimes that make triplet states easily depopulated through vibrational effects, at least in purely organic molecular designs.

Still, some examples of thermometry can be found using phosphorescent organic molecules, by embedding them in glassy polymer films that help suppressing vibrational quenching [43]. However, most of the organic dyes used in thermometry are fluorescent, such as rhodamine B or fluorescein, since their emission intensity and lifetime vary with temperature. A representative example was provided by Ross et al., who used the intensity of rhodamine B in water to study temperature gradients generated by applying a voltage difference between the two ends of a microfluidic channel (**Figure 5**) [44]. In this experiment, the channels were placed in a standard fluorescence microscope and illuminated with a mercury arc lamp. Luminescence was then detected with a CCD camera capable of time-resolved 2D mapping, even for times shorter than a second, so that the spatial resolution of the thermal gradient could show the asymmetry created by the direction of a generated electroosmotic current (from left to right in the figure).

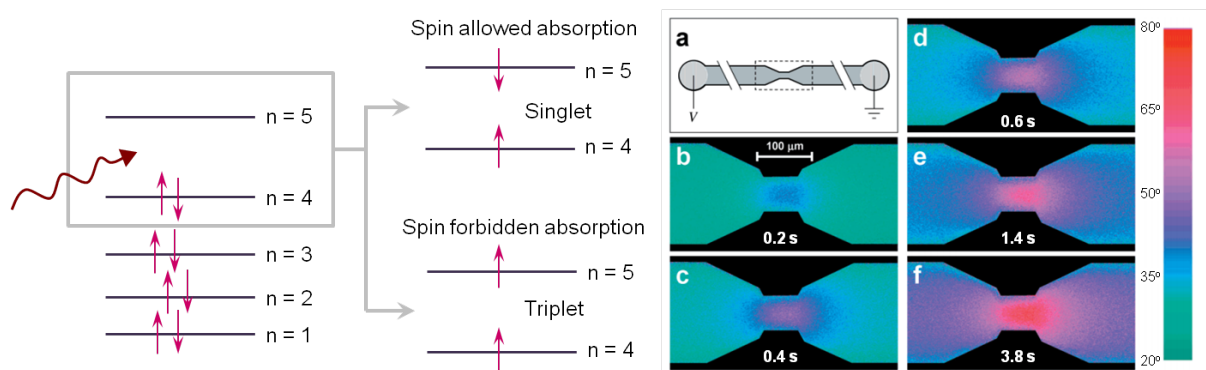


Figure 5. Left: Schematic energy diagram showing two localized excited states of organic dyes that result in fluorescence (if the excited state is a singlet) or phosphorescence (if the excited state is a triplet). Right: thermal distribution in a microfluidic channel with a potential applied to its ends. Temperature was measured by monitoring fluorescence intensity of rhodamine B. Adapted with permission from the American Chemical Society from Ref. [44].

In this example the intensity of the dye is reduced when the temperature is raised, as it usually happens in organic dyes due to an increased contribution of non-radiative transitions at higher temperatures. Since the relationship between intensity and temperature is non-linear, the

sensitivity of the sensor (from equation (1) it is given by $\partial I/\partial T$, where I is the intensity) is temperature dependent. In particular, it is higher closer to room temperature than above it. This affects the accuracy of the measurement, though accuracy depends as well on how fluorescence is recorded during the experiment. For instance, in the results shown in **Figure 5** the thermal resolution was 2.4 °C close to room temperature but 3.5 °C at 85 °C. Yet, if fast acquisition is not required and thus averaging over time is possible, the thermal resolution obtained in this work was as low as 0.03 °C at room temperature and 0.07 °C at 85 °C. This strategy is thus valid for the study of fluids in microchannels and has indeed been applied for different types of structures such as cross-slot microgeometries [45], temperature-jump chips [46], or herringbone structures designed to enhance heat transfer [47], but it also has certain limitations that need to be considered. On one hand, the intensity recorded is affected by fluctuations of the illumination source, photobleaching, or inhomogeneous dye concentration. Indeed, Ross et al. mentioned that the dye was to some extent adsorbed onto the channel walls, and thus the measurements were carried out with a sufficiently high concentration of Rhodamine B so that the volume of adsorbed dye was negligible [44]. On the other hand, the fluorescence intensity and lifetime of organic dyes not only depends on temperature, but can also change due to pH variations or other changes related to the solvent. Accordingly, if the application requires a more complex environment the thermal probe should be adapted [48].

A solution to the problem related to fluctuations of the illumination is the simultaneous use of two different dyes with differentiated thermal sensitivity and emission wavelengths. In this approach rhodamine B (sensitivity $\sim 1\%K^{-1}$) is typically mixed with another dye featuring very low or negligible thermal sensitivity, such as rhodamine-110, rhodamine-560 or sulforhodamine-101, which can be used as a reference [49]. However, the sensitivity can still be enhanced if the

emission intensity of the second dye increases with temperature, rather than decreasing. For this reason, few studies have optimized the use of fluorescein-27 which, at certain excitation wavelengths, presents an increase in fluorescence with temperature due to a thermally-dependent shift of the absorption curve, reaching a sensitivity of the mixture of $7\%K^{-1}$ [50, 51]. Following this approach, a lack of control on the illumination is no longer a problem, but using two different dyes immediately raises an additional issue: the concentration of both molecules needs to be spatially controlled all along the experiment. Such limitations can be resolved by trapping both dyes together in a single structure. This strategy has been applied to *in vivo* thermal imaging in fruit fly larva, using polymeric spheres with two different fluorophores embedded (Eu-tris(dinaphthoylmethane)-bis-trioctylphosphine oxide as thermal sensitive fluorophore and tris(2-phenylpyridinato-C2, N) iridium(III) as reference) [52]. The larvae were observed after oral administration of the spheres using a conventional epifluorescence microscope under 390 nm excitation and recording the luminescence between 490 – 690 nm. This presents the advantage of being a technique that can be easily exported to different laboratories. However, this advantage is also limiting the application of the structure to small transparent organisms, since visible light is largely absorbed by biological tissues, and requires the administration of a sufficiently high concentration of particles to obtain a luminescent signal that can overcome tissue autofluorescence. In order to avoid autofluorescence, the same group reported the exchange of the Ir(III)-complex by rhodamine 800, which resulted in shifting the reference signal to the near-infrared range (though the thermometric signal still remained in the visible). The performance of the resulting thermal probes in the form of polymer particles [53] or polymeric sheets [54] was tested in living beetles with the covering cuticles partly removed.

When organic molecules are close to each other (typically at distances below 1 nm), it is possible to create bimolecular excited states between an excited molecule and another molecule in its ground state, as long as they have resonant energy levels. Such a combination is called an excimer (or exciplex if both molecules are of different species) and is responsible for distinct emission bands, which are broader and blue-shifted with respect to the emission bands of the isolated molecule. A consequence of excimer formation is that the solution would present two different emission bands that can be used as reference and probe in a thermometer design [55], showing sensitivities as high as 4.5 %K⁻¹ [56]. Molecular interactions can thus be exploited in thermometry, though again, as more than one molecule is involved, tight control over concentration is important, in particular when both molecules are different.

We have discussed so far options based on luminescence intensity or lifetime changes, but alternative strategies involving organic molecules are also available. An interesting option relates to so-called twisted intramolecular charge transfer (TICT) compounds, whose intensity remains fairly constant within a wide temperature range, but undergo emission shifts, leading to colorimetric temperature sensing (see **Figure 6**). This behavior arises from the emission of the compound comprising various contributions related to either the local states of the molecule (singlet or triplet) or to intramolecular charge-transfer bands. The weight of each contribution to the observed emission changes upon conformational changes of the molecule, which can be triggered upon heating. However, it should be noted that environmental changes in polarity or viscosity may also modify the rate of these changes and hinder thermal reading. Interesting examples of such colorimetric thermometers were presented by Yang and colleagues, using triarylboron-based compounds in solution [57], within microcapsules [58] or in a solid-state polymer (**Figure 6**) [59].

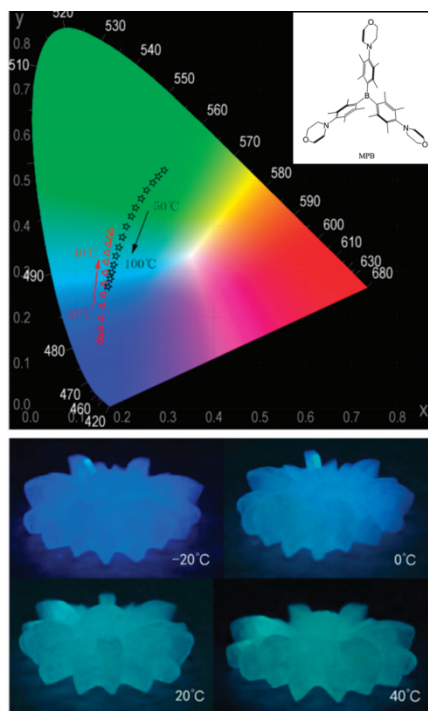


Figure 6. Example of colorimetric changes of a TICT dye based on a triarylboron compound (inset). The upper CIE diagram shows the evolution of emission color with temperature, when the triarylboron compound is in a 2-methoxyethylether solution (stars) or embedded in a solid PEG-4000 polymer (triangles). The lower images present the aspect of a silica gel at different temperatures, when excited with UV light at 335 nm. Adapted from Ref. [59] with permission from The Royal Society of Chemistry.

The sensitivity of the fluorescence of organic molecules toward solvent properties such as polarity, viscosity or ionic strength, not only to temperature, together with the occasional need to control their spatial distribution, triggered the development of several strategies toward controlling the direct environment of the fluorophore, e.g. incorporating the organic dye in a glass or a gel [60]. The resulting thermometric film cannot be introduced inside a micrometric environment but can be used as a working surface that provides information on temperature, with spatial resolution limited by film quality [61]. Alternatively, dyes can be encapsulated within micelles, which would reduce contact of the dye with the environment while keeping the particulated structure of the thermometer. A demonstration has been provided by Wu et al., who

co-encapsulated rhodamine B and rhodamine 110 in polymeric micelles, resulting in a system with luminescence independent of pH, ionic strength and solvent viscosity, but maintaining a thermal sensitivity of $7\%K^{-1}$ [62].

Even though in these examples polymers act as passive scaffolds containing the dye, they can also be specifically designed to actively participate in the thermometer design. This is the case of thermoresponsive polymers, i.e. polymers that undergo a reversible phase transition linked to temperature. The polymer transitions from a coil state in water (hydrophilic) to a dehydrated state (hydrophobic) in which the polymer chains collapse forming a globule, leaving most water molecules outside. As a consequence, dye molecules that stay inside the polymeric globule effectively see a different local environment, thereby presenting a distinct luminescent response (**Figure 7**). Due to temperature-dependent molecular interactions (hydrogen bonding and hydrophobic attraction), most thermoresponsive polymers applied in thermometry form the globule state above a certain transition temperature, which is known as lower critical solution temperature (LCST). Some polymers however display a reverse behavior due to stronger inter-polymer attraction at lower temperatures, and then the transition temperature is called upper critical solution temperature (UCST) [9].

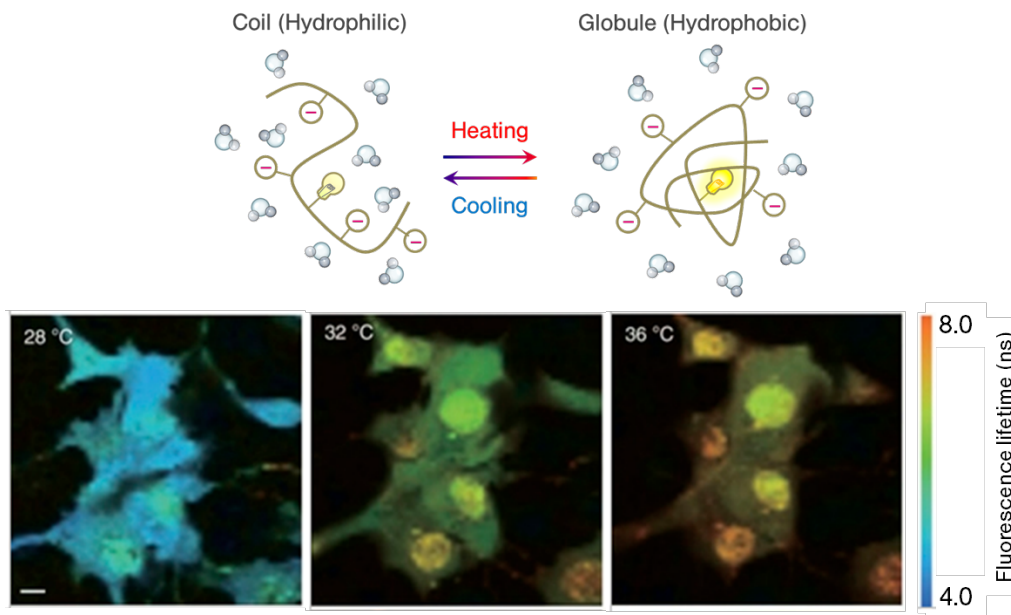


Figure 7. Upper panel: scheme showing the behavior of an LCST thermoresponsive polymer. Lower panel: False color images showing the different lifetimes of NNPAM modified with a fluorescent unit (DBD-AA) located in externally heated COS7 cells. Adapted by permission from Springer Nature, Ref. [16]. Copyright 2012.

The phase-transition of LCST polymers typically occurs within a narrow temperature range (typically $\Delta T \sim 5 - 10$ °C), where they boost the thermal sensitivity of the embedded dye. The transition of UCST polymers instead, happens within a broader thermal range. This would in principle be an advantage for thermometry design with increased sensitivity over a wider temperature range. Nevertheless, likely because polymers with UCST transitions are rarely water soluble, most thermometers are based on LCST polymers [9]. Some examples based on UCST have been reported, such as the thermometer designed by Pietsch et al. using PMMA as UCST polymer, combined with a solvatochromic dye, with intensity linearly decreasing between 10 and 35 °C [63].

The most popular LCST polymer in nanothermometry (and other applications) is poly(N-isopropylacrylamide), PNIPAM, since it is water soluble, displays weak pH dependence and low

toxicity, with a transition temperature around 32 °C, in the range of the biological temperatures of interest. On the negative side, vitrification may occur at high polymer concentration upon heating, partially affecting the reversibility of the transition [64]. In this respect, poly(oligoethylene glycol (meth)acrylate), POEG(M)A, appears as an advantageous alternative that can also be easily modified by adding different monomers to form a co-polymer with tailored transition temperature. This possibility has been demonstrated in the range between 28 and 81 °C [65]. An example of application was provided by Okabe et al., who modified the thermoresponsive poly-*N-n*-propylacrylamide (NNPAM) with a fluorescent unit to build a thermometer with no dependence from environmental pH or ionic strength. Instead of using the intensity of the fluorophore as a probe, fluorescence lifetime was monitored to minimize the potential contributions from concentration inhomogeneities. Due to the low toxicity of the system and its reduced size (9 nm hydrodynamic diameter in the globular state), it could be incorporated in living cells (nucleus and cytoplasm) to monitor their temperature (**Figure 7**). The authors presented intracellular temperature maps with diffraction-limited spatial resolution and thermal resolution between 0.3 and 0.6 °C, seeing thermal differences (≤ 1 °C) between the nucleus, centrosomes, mitochondria and cytoplasm, which were attributed to thermogenesis [16].

An additional aspect regarding the fluorescence of organic molecules toward thermometry and in particular intracellular thermal mapping is the anisotropy of the polarized emission. Luminescent molecules excited with linearly polarized light emit partially polarized light depending on the orientation of their dipoles which in principle is random. Polarization anisotropy, r , can be defined as the ratio between the intensity of the two possible output polarizations: parallel, I_{\parallel} , or perpendicular, I_{\perp} to the excitation polarization [66].

$$r = \frac{I_{\parallel} - I_{\perp}}{I_{\parallel} + 2I_{\perp}} \quad (5)$$

At rest, r would take its maximum value of 0.4, but molecular rotation related to Brownian motion decreases the measured value of r , defined by

$$\frac{1}{r} = \frac{1}{r_0} \left(1 + \frac{\tau_F}{\tau_R} \right) \quad (6)$$

where r_0 is approximately 0.4, τ_F is the fluorescence lifetime and τ_R the rotational relaxation lifetime that can be given, following Debye-Stokes-Einstein equation, by $\tau_R = V\eta/K_B T$, V being the hydrodynamic volume of the molecule, η the viscosity of the solvent, K_B Boltzmann's constant and T the temperature. This equation means that fluorescence depolarization depends on how fast molecules rotate compared to the time that they take to emit light. Since rotational lifetime is temperature dependent, r can be used as a temperature sensor [67]. A temperature measurement based on this technique is free from inaccuracies due to the inhomogeneous fluorophore distribution, fluctuations in illumination or photobleaching, because it is a ratiometric approach. It should however be noted, that polarization anisotropy has a complex dependency on temperature since both fluid viscosity and fluorescence lifetime may also depend on it. Accordingly, either these dependencies are taken into account when the thermometer is calibrated or molecules are specifically selected to minimize these contributions [68]. For example, Baffou et al. applied this technique to measure the heat generated by gold nanorods, using fluorescein as the organic dye, a molecule with high fluorescence lifetime stability in the considered thermal range (~ 4 ns) [67]. The choice of the solvent was motivated by equation (6) and the Debye-Stokes-Einstein equation, which show that the sensitivity of the thermal sensor increases with the viscosity of the medium. In particular, in the designed experimental scheme, a thermal resolution of 0.1 °C was achieved (see scheme in **Figure 8**). In a latter work from the

same group, the technique was exported to intracellular thermal imaging, where the viscosity of the medium cannot be tuned. Consequently, in order to obtain sufficient thermal sensitivity, they increased the hydrodynamic volume of the fluorophore by using the green fluorescent protein (GFP), which has a characteristic size of 3.5 nm and a rotational correlation time, τ_R , which happens to be in the same order of magnitude of its fluorescence lifetime. In order to create a thermal gradient, they incorporated gold nanorods to the extracellular medium, which act as external heaters upon illumination. In the obtained intracellular images, they obtained a thermal resolution of 1.4 °C. The spatial distribution of GFP inside the cells was inhomogeneous and consequently the emission maps showed areas with higher and lower intensity. However, since polarization anisotropy is a ratiometric technique, such intensity differences in fluorophore emission do not have a detrimental effect in the accuracy of the thermal measurement (**Figure 8**) [69]. This technique has also been successfully applied to *in vivo* experiments by incorporating GFP expressing neurons to the semi-transparent nematode *C. Elegans* [70]. However, the technique is limited due to the high extinction cross section of biological tissues in the visible, where all the fluorophores tested so far operate, thereby limiting its use to small transparent animals.

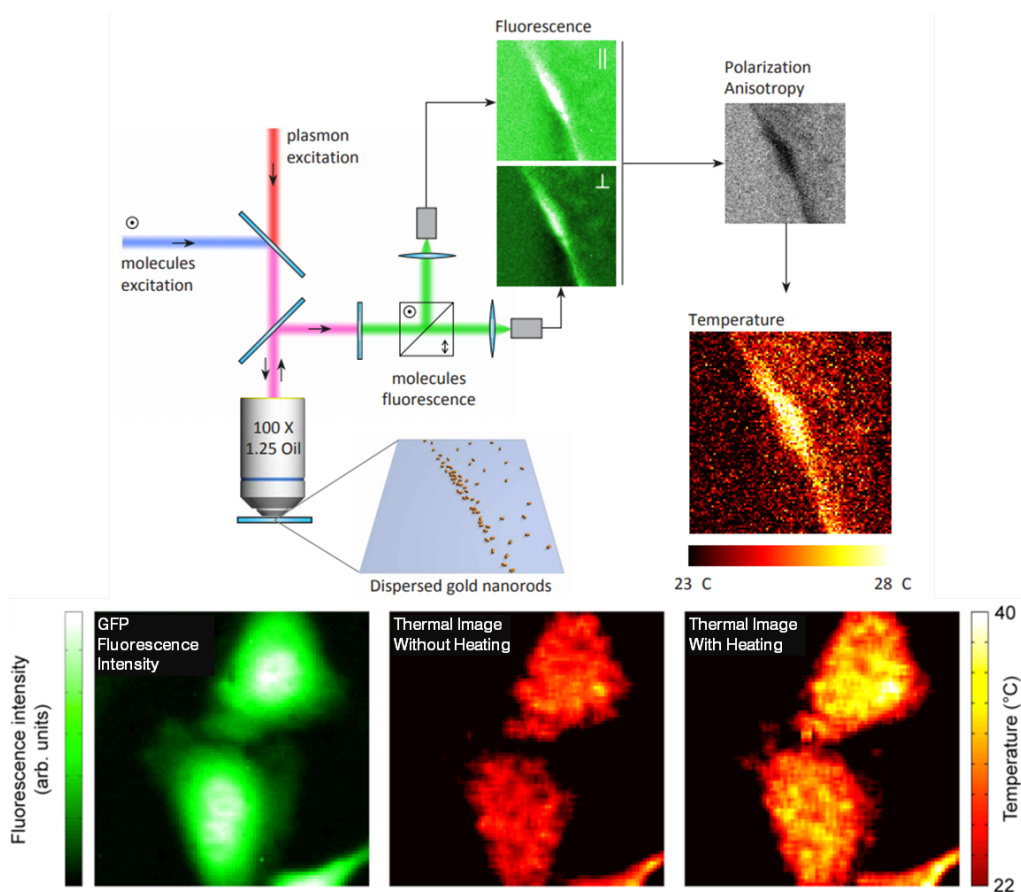


Figure 8. Upper panel: Experimental set-up used to measure temperature from the polarization anisotropy of fluorescein. The sample comprises a layer of optically excited gold nanorods to act as heaters. Maps were recorded with both light polarizations and then combined to plot temperature (Reprinted from Ref.[67]. Open access). Lower panel: GFP is internalized by HeLa cells to measure intracellular temperature through polarization anisotropy. The first map shows the inhomogeneous intensity distribution of GFP. The following images are thermal maps at two different temperatures. The distribution of intensities does not interfere with the thermal reading, thanks to being a ratiometric technique. Reprinted with permission from Ref. [69]. Copyright 2012, American Chemical Society.

5.2. Quantum Dots (semiconductor nanoparticles)

One of the key examples of size effects for nanoscale materials is the confinement of electrons and holes in semiconductors, which render quantum dots suitable fluorescent probes for multiple applications, including nanothermometry. Semiconductors display a valence band filled with electrons and a conduction band separated from the valence band by an energy gap. This

energetic distance is enough to keep electrons in the valence band, some of these electrons can be promoted to the conduction band upon excitation with photons of larger energy than the gap. This electronic promotion leaves a hole in the valence band, which behaves like a particle with positive charge. When the characteristic energy of the excitation light is just below the bandgap energy, electron and hole can remain bound through Coulomb interaction, forming what is called an electron-hole pair or exciton [71]. Excitons have important implications regarding luminescence in semiconductor nanostructures, as it is their recombination what involves the emission of a photon and thus, luminescence. Excitons can be assigned a size, a_B^e , called exciton Bohr radius, which depends on the dielectric constant of the semiconductor crystal, ϵ , and the effective mass of the exciton, μ , through the expression $a_B^e = \epsilon(m_e/\mu)a_B$; where m_e is the mass of the electron and a_B the Bohr radius. This means that the size of the exciton is not defined by the Coulomb interaction, but by the properties of the semiconductor material. Quantum confinement effects in quantum dots are observed when the radius of the dot is smaller than the exciton Bohr radius, which depending on the material can be in the nanometer range, as is the case of II-VI cadmium-based dots, or tens of nanometers, as is the case of IV-VI Pb-chalcogenides [72]. When excitons are confined in a quantum dot, discrete energy states appear in its energy structure (**Figure 9**), which are linked to absorption peaks and make optical transitions possible. As the number and energy of these states depend on the size of the quantum dot, so do its absorption and emission spectra.

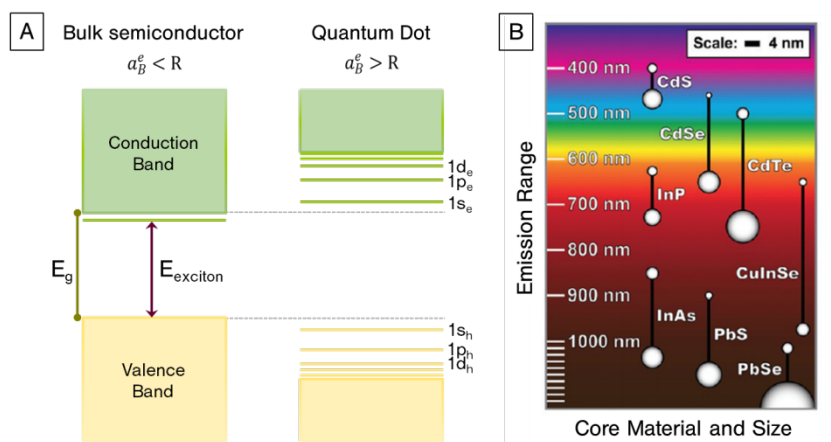


Figure 9. (A) Scheme comparing the distribution of energy states of a semiconductor with a radius R , larger than the exciton Bohr radius, and a semiconductor with a radius smaller than the exciton Bohr radius. In the latter case, discrete levels form within the energy gap due to carrier confinement. (B) Diagram showing the emission wavelength of quantum dots with different diameters and made of different materials. Reprinted with permission from Ref. [73]. Copyright 2011, American Chemical Society.

When used as luminescent probes, quantum dots benefit from the possibility to tune the emission wavelength along the visible and near-IR ranges by simply changing particle size and composition (**Figure 9B**). Additionally, photobleaching is significantly reduced, rendering quantum dots suitable candidates as fluorescent labels. A drawback for certain applications is their characteristic blinking, meaning that the emission intensity is not constant over time. However, this is only a limitation if the study requires measuring the emission of a small number of quantum dots, but the impact of blinking becomes negligible if a larger concentration of particles can be used. On the positive side, the luminescence quantum yield of quantum dots is often rather high (above 50%, in some cases reaching 80% or 90%) [74], which is a great advantage for sensing, as bright signals facilitate getting a good thermal resolution. For biomedical applications though, the main concerns arise regarding potential toxicity, due to the presence of heavy metal ions such as lead or cadmium, which are considered highly toxic. Although this issue has been largely addressed, discussion continues [75] and an agreement has

not been reached because many different parameters affect toxicity, so a full study is required for each type of quantum dots. Indeed, a recent meta-analysis study including information from 307 publications on cellular toxicity of the most common quantum dots based on cadmium (CdSe and CdTe) states that between seventeen attributes of quantum dots considered, toxicity closely correlates with diameter, concentration, surface ligand, exposure time, surface modification, type of assay, as well as with the presence of a shell that may prevent cadmium from leaching out of the core [76].

Coming back to thermal sensing, a number of properties of the emission by quantum dots are affected by temperature, including intensity, lifetime, peak position and Stokes-shift (spectral separation between absorption and emission). In general, the emission intensity of a fluorophore is the simplest option to determine temperature, upon calibration. However, the recorded intensity not only varies with temperature, but also with particle concentration and fluctuations on the excitation power, and thus in practice it can only be used in stable situations where concentration remains constant. Still, the emission intensity of quantum dots depends on temperature and it has been exploited in nanothermometry. It is actually advantageous in situations in which absolute temperatures are not as important as determining a thermal increment over a period of time. In these cases, the concentration of particles is no longer an issue (as long as it remains constant during the experiment) and the simplicity of the technique becomes an asset. This is the case of the work of Laha et al., where CdTe quantum dots were used to determine the efficiency of skeletal muscle *ex vivo*, by measuring transient thermal changes, triggered by the addition of adenosine trisphosphate (ATP) [77]. Another interesting application is the detection of ischemia, which has been tested *in vivo* by injecting near-infrared emitting quantum dots (PbS/CdS/ZnS) into mice [78]. In this work, the diagnosis was based on a

technique called Transient Thermometry (TTh) in which the studied tissue is first heated up and then its thermal recovery profile is recorded and analyzed to determine its health status.

Typically, the emission intensity of a fluorophore is linked to temperature via the interaction with phonons through electron-phonon coupling (**Figure 10A**) or multiphonon transitions (**Figure 10B**), but the variation is negligible in quantum dots. Instead, the intensity quenching observed in quantum dots when temperature is increased has been related to the existence of trap states or defects associated to the surface of the dot [79-81]. The suggested mechanism involves the escape of a carrier to a nearby trap or surface defect state, becoming unavailable to contribute to the luminescence of the dot. The thermal dependence of intensity would then follow that of the trap (or defect) states. From the thermal sensor point of view, this involves two main limitations. One is that the thermal dependence of the dot intensity changes with the nature of its surface and the environment, and accordingly the sensor must be calibrated for each specific case. The second limitation is that in many systems thermal quenching is not fully reversible, meaning that the luminescence intensity recorded at a certain temperature during a heating experiment can be higher than that recorded at the same temperature when cooling down (**Figure 10E**) [80]. Such partial irreversible quenching occurs only if a certain threshold temperature is surpassed. In the case of CdSe/CdS/ZnS quantum dots, it was found that this threshold is between 100 and 160 °C (**Figure 10E**). However, irreversibility below 100 °C was found for CdSe/CdS, and does not seem to exist in CdTe/CdSe. The reasoning behind the existence of reversible and irreversible quenching based on traps (**Figure 10C,D**) relies on different types of traps or defects. For instance, high temperature may induce structural defects related to interfacial strain and core-shell mismatch, which may become permanent – accounting for irreversible quenching – or be temporary, whereas pre-existing surface defects would justify

reversible quenching only. As shown in **Figure 10E**, the luminescence lifetime of quantum dots also changes with temperature and can be related to trap states. Quantum dots would thus also be a limited system to measure temperature through lifetimes. It must be noted at this point that intensity measurements are advantageous because of their simplicity whereas lifetime determination is generally a more complex experiment. However, lifetimes are free from the influence of quantum dot concentration, as well as from variations in the light excitation power. Therefore, lifetime becomes an interesting parameter in those cases where no irreversibility is observed. Indeed, it has been exploited to study the heating of a suspension of CdTe quantum dots in water due to laser illumination [82].

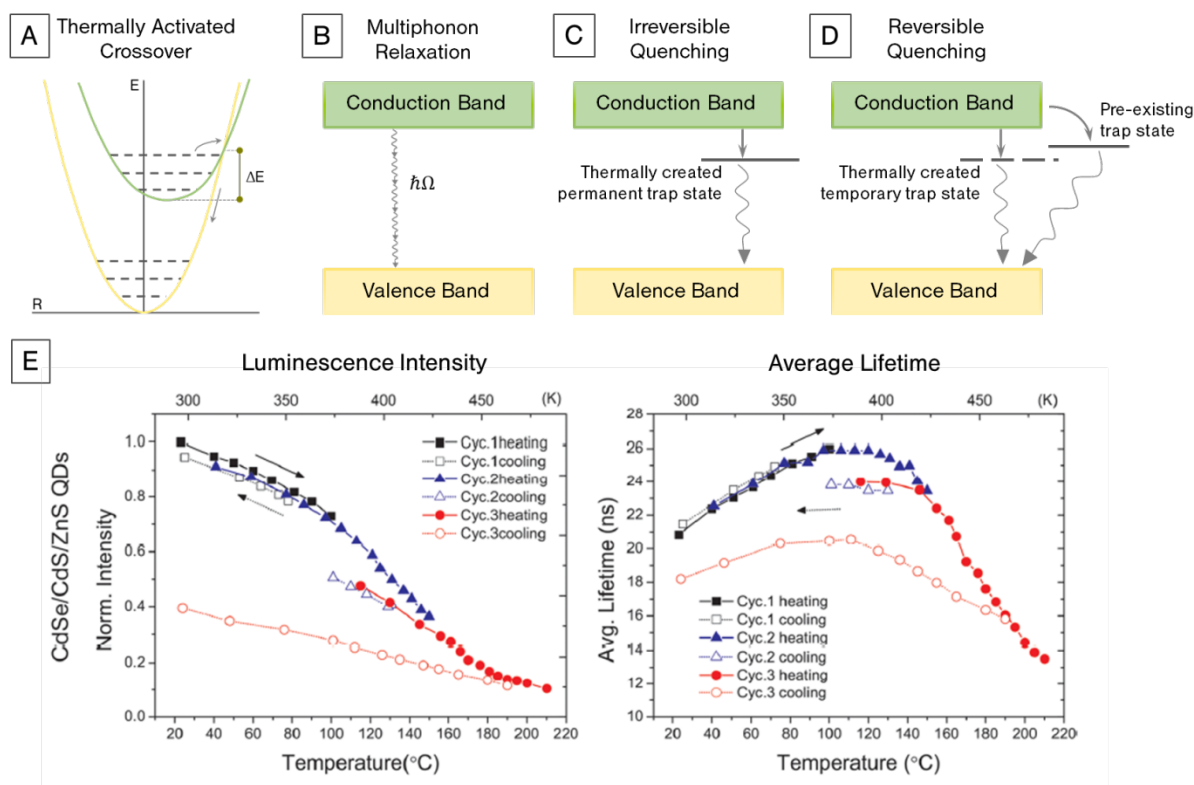


Figure 10. Schemes showing different quenching mechanisms for quantum dots: (A) thermally activated crossover, (B) multiphonon relaxation, (C) irreversible quenching, and (D) reversible quenching. (E) Normalized luminescence intensity and lifetime for CdSe/CdS/ZnS quantum dots exposed to several heating/cooling cycles, to determine the temperature at which the process

becomes irreversible. Reprinted with permission from Ref. [80]. Copyright 2012, American Chemical Society.

Aside from intensity and lifetime, the most usual quantum dots parameter applied for thermometry is the shift of the emission peak [7, 72]. Due to a combination of factors, the emission shift due to a temperature increase changes depending on the particular quantum dots, through size and composition, to the extent that it can be either a blue-shift or a red-shift. The factors involved in the wavelength shift include material expansion, and the associated size variation has an effect on exciton confinement, which is reflected as a red shift of the emission wavelength. At the same time, the interatomic distances in the dot lattice also change, affecting the exciton energy and resulting in a blue shift of the emission, which opposes the effect caused by thermal expansion (**Figure 11**). Additionally, electron-phonon coupling is also affected by temperature. In this case, we can differentiate two components depending on whether the coupling is with electron-electron and hole-hole states (interband) or with electron-hole states (intraband). Each electron-phonon contribution affects again in a different way (**Figure 11**), since interband coupling would induce a blue-shift of the emission with temperature, while intraband coupling would produce the opposite effect. Olkhovets et al. used PbS and PbSe quantum dots of different sizes in different materials (phosphate glass, oxide glass and polymer) to study this thermal behavior [83]. They plotted the change of the energy gap, E_g , with temperature for a set of quantum dots with different sizes (**Figure 11**) and observed that summing up all the contributions, the final result is dependent on the dot's size. In the case of PbS and PbSe (IV-VI semiconductors with large Bohr radius), the larger dots present a blue shift when temperature is increased, while the smaller ones present a red shift. The authors claim that this behavior, as well as dE_g/dT calculated values – directly related to the thermal sensitivity (equation (1)) – depends on the material. For example, in II-VI semiconductors such as CdS or

CdSe, intraband electron-phonon terms are much larger than interband electron-phonon terms, resulting in $dE_g/dT < 0$.

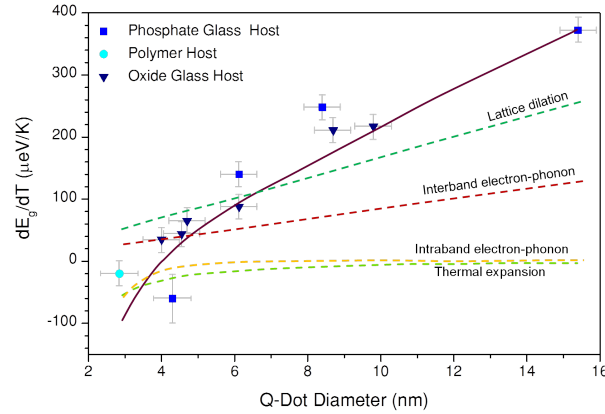


Figure 11. Energy gap variation with temperature (dE_g/dT) for PbS quantum dots with different sizes. The measurements were made with quantum dots in different media, including phosphate glass, polymer and oxide glass. The dashed lines are a calculation of the expected trends due to the different contributions affecting dE_g/dT [83].

Several works have used the dependence of the shift to obtain practical information on temperature at the nanoscale, either for materials characterization [84] or biomedical applications. A particularly interesting example of this last category is the study of Martínez-Maestro et al., on the thermometry properties of 4 nm CdSe quantum dots [85]. The authors observed that both emission intensity and peak shift can potentially be used for thermometry. The quantum dots were first excited at 488 nm with a continuous-wave laser, thus following a standard excitation/emission scheme, but they also used an 800 nm femtosecond-pulsed laser to achieve emission via multiphoton excitation. In this way they observed that the peak wavelength was red-shifted when increasing temperature, at a rate of 0.16 nm/K, regardless of the excitation scheme. This means that the sensitivity of the thermometer is a robust parameter, independent of the excitation scheme. On the contrary, the sensitivity of a thermometer based on intensity does

depend on the excitation scheme, ranging from 0.83 %K⁻¹ with 488 nm excitation to 2.5 %K⁻¹ for multiphoton excitation. This suggests a thermal dependence on the absorption cross-section of the material that gets amplified when using a multiphoton excitation scheme. Interestingly, the authors combined both thermometry options to measure temperature, first due to laser heating by focusing a 980 nm beam on a cuvette, and then in externally heated HeLa cells containing internalized quantum dots.

Following the biomedical applications perspective, the work of Martínez-Maestro et al. [85] is also an interesting proposal because multiphoton excitation schemes present advantages such as reduced heat delivery to the sample. The absorption cross-section of biological tissue is high in the visible but gets lower at the near-IR. Indeed, three wavelength ranges are typically defined as biological transparency windows for light-based biological applications: 750-950 nm; 1000-1450 nm, and 1500-1700 nm. By working within these wavelength ranges the heat delivered to the biological sample is reduced, which is important from both the thermal accuracy and the sample survival points of view, but it also presents some other advantages. For instance, penetration depth *in vivo* is improved and, very important, autofluorescence is reduced resulting in improved contrast and easier to interpret images [86]. Full benefit from these advantages can however only be obtained if the emission also lies within the biological windows. Fortunately, recent developments in quantum dot design also offer emission within this range (**Figure 9B**), even allowing for *in vivo* experiments, such as the above mentioned case of ischemia detection in mice through the thermal relaxation of tissues [78].

Considering all the presented information, it is clear that quantum dots constitute a suitable option for nanothermometry. However, important limitations arise from variations of luminescence parameters (intensity, lifetime and spectral shift) with the environment, including

surfactants and ligands. This can be a source of error in thermal readings if the sample is not properly calibrated for the application, but it can potentially be exploited to design better thermometers, since a smart choice of coating can help improving the sensitivity of the quantum dots, or increase their stability during heating/cooling cycles [72].

5.3. Lanthanide-based nanothermometers

Lanthanide ion-doped nanoparticles are a specific family of optical materials that can be designed to emit light in the UV, visible or near-IR ranges. This category of materials comprise a transparent host, often a crystal, which is doped with a certain concentration of lanthanide ions to incorporate their energy states to the crystal gap, providing it with highly specific optical properties. Such properties arise from partial filling of orbital $4f$ in the lanthanides family, while the less energetic $5s$ and $5p$ orbitals are full. However, $4f$ is closer to the atomic nucleus than $5s$ and $5p$ and thus its electrons are shielded from the outside [87]. Since the luminescence of lanthanides is related to transitions within $4f$ states, this shielding implies that their absorption and emission bands are weakly influenced by the environment, and as a result they are typically narrow and formed by sets of well-defined peaks. The crystal environment however plays an important role in the luminescence of lanthanides, since the electronic transitions between $4f$ energy states are partially forbidden according to the selection rules, but they become partially allowed when the lanthanide feels an asymmetric field. In the case of a crystal doped with lanthanides, this field is provided by the atoms forming the crystal lattice, and is thus known as crystal field [88]. **Figure 12** schematically shows the degeneracy breaking of the energy states of lanthanides as a source of their characteristic luminescence, including the order of magnitude of the energetic separation between sublevels, ΔE , which is related to the sensitivity of some thermometers.

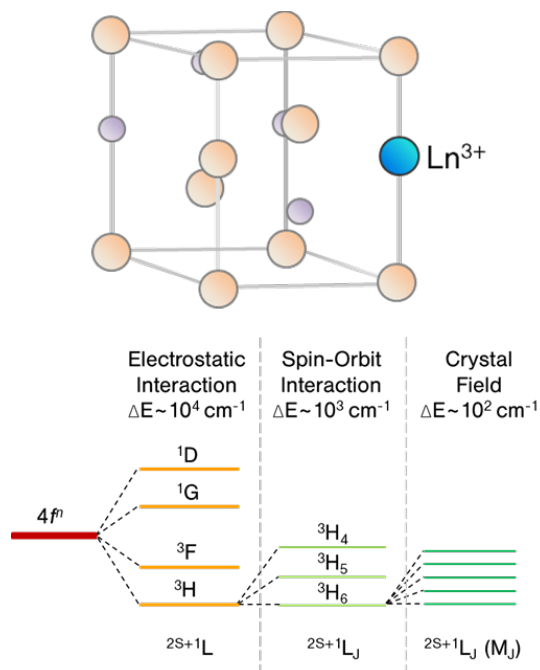


Figure 12. Example of unit cell of a material doped with a lanthanide ion (Ln³⁺). As a consequence of the incorporation to a crystal lattice, there is a certain degree of level splitting. The lower scheme shows the different contributions to the splitting and how the energy states are labeled accordingly.

Each lanthanide ion possesses a set of energy states that is only weakly modified within the crystalline environment and thus, it becomes its luminescent fingerprint (see **Figure 13** for an example of energy diagram and corresponding emission spectrum) [89]. As optical probes, lanthanide-doped materials present significant advantages, as their luminescence is easy to identify and differentiate from other materials; emission bands are narrow facilitating multiplexing; and can be easily predicted, allowing complex designs specifically developed for each application. As a main drawback, the absorption cross-sections and quantum yields of lanthanide-doped nanoparticles are typically lower than those from other luminescent probes, and often need to be compensated by higher excitation power or longer detection time.

Each lanthanide energy state has an absorption band and an associated emission band (unless the next lower-lying state is energetically close so electrons can get non-radiatively relaxed into it),

and all of them can be potentially used to sense temperature. This provides a wide range of excitation and emission wavelengths to select, depending on the experiment. For example, in the case of erbium, as shown in **Figure 13B,C**, after excitation into the $^4F_{7/2}$ state (typically with a wavelength around 480 nm) it would be possible to observe emissions from $^2H_{11/2}$ and $^4S_{3/2}$ in the green range (typically between 520 – 560 nm), from $^4F_{9/2}$ in the red (typically ~660 nm), and from $^4I_{11/2}$ and $^4I_{13/2}$ in the near IR (~980 nm and ~1520 nm, respectively; not shown in the figure).

However, what makes lanthanide ions outstanding for luminescence is the additional possibility to obtain light emission with shorter wavelength (larger energy) than the excitation. The involved mechanism, known as upconversion, deserves special attention here, since it provides an advantage for multiple applications. In e.g. biological samples studied *in vitro*, this excitation mechanism would prevent autofluorescence and thereby increase image contrast and reduce noise. It is possible to get upconverted emission from materials doped with only one lanthanide element, such as Er^{3+} or Tm^{3+} , through excited state absorption or energy transfer between ions of the same species. However, materials are often co-doped with two different lanthanide ions (**Figure 13A**) to improve both the upconversion quantum yield and the absorption cross-section. In such cases, one of the dopants is specifically selected to behave as an antenna for the excitation light, Yb^{3+} most often playing this role. The second dopant is selected to capture the energy absorbed by the first one through energy transfer and subsequently emit photons of shorter wavelength. A good example of an upconversion system, with important applications in thermometry, is the co-doping with Er^{3+} and Yb^{3+} ions. In this case, Yb^{3+} ions absorb near-IR 980 nm radiation, which is then re-emitted by erbium ions mostly in the green and red spectral ranges. The simplified upconversion mechanism in Er^{3+} , Yb^{3+} systems is shown in the energy

level diagram of **Figure 13B**. The overall mechanism is based on energy transfer between both ions, which takes place because the energy gap between the ground state of ytterbium and its first (and only) excited state, is equal to the gap between several energy levels of Er^{3+} (resonant transitions marked with grey arrows in the Er^{3+} diagram). Accordingly, Er^{3+} gets excited by Yb^{3+} through energy transfer, first from the ground state to $^4\text{I}_{11/2}$. Then, since the lifetime of lanthanide energy states is rather long (typically in the millisecond range), it is possible that more equivalent energy transfer steps (red arrows) take place from excited states, progressively populating the upper excited levels, which can emit at shorter wavelengths. **Figure 12C** shows the emission spectrum of $\text{NaGdF}_4:\text{Er}^{3+},\text{Yb}^{3+}$ upon 980 nm laser excitation.

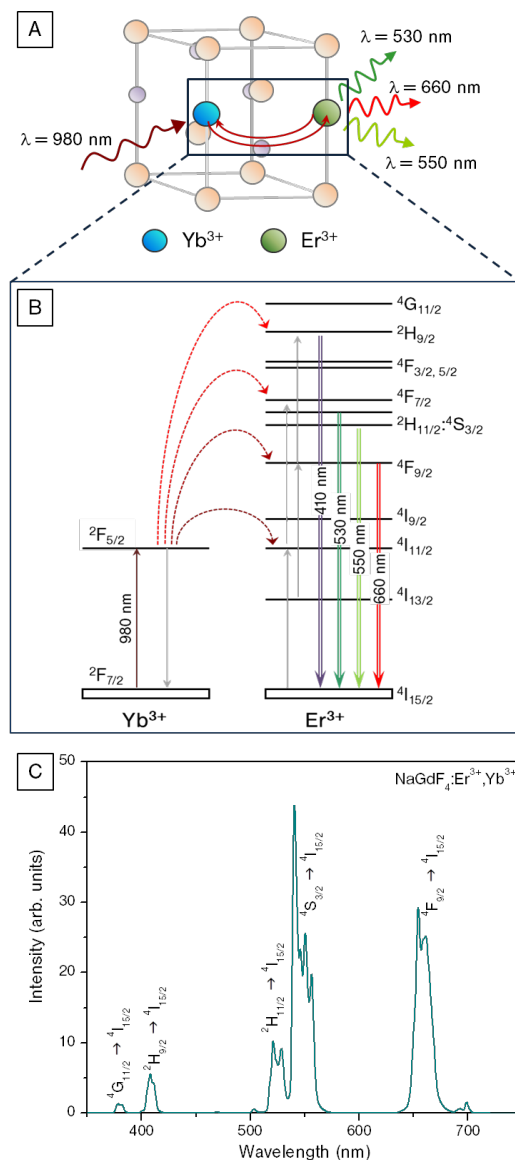


Figure 13. (A) Representative crystal doped with two lanthanide ions, Er³⁺ and Yb³⁺. As a result of their interaction, upconversion processes are possible, and upon 980 nm excitation a set of visible emission bands are observed, the most intense ones at 660 nm, 550 nm and 530 nm. (B) Simplified upconversion mechanism schematically shown in a partial energy diagram of an Er³⁺,Yb³⁺-doped system. The red arrows indicate energy transfer processes between both ions, and the grey ones indicate transitions that are resonant with Yb³⁺ relaxation. (C) Typical emission spectrum obtained from a solution of NaGdF₄:Er³⁺,Yb³⁺ nanoparticles. The spectrum was obtained with 980 nm excitation, and shows the resulting visible emission bands.

Regardless of the excitation scheme, the emission bands of lanthanide ions incorporated to a crystal host are not affected by most environmental parameters, but depend on temperature in

different ways. In general, when temperature is increased, the various emission peaks get wider due to homogeneous broadening (related to lattice vibrations), the overall intensity of the spectrum decreases as non-radiative (assisted by lattice phonons) relaxations become more likely, and for the same reason the lifetimes of radiative transitions become shorter. Any of these characteristics can be used to define a thermometer using lanthanide-doped nanoparticles, and all of them have been proposed and tested [10].

Bandwidth is a convenient parameter that can hardly be altered by changes in the nanoparticle environment, aside of temperature. However, the relationship between bandwidth and temperature is not always simple and it does not necessarily follow a uniform trend within a wide temperature range. Additionally, changes are rather small and often require the use of spectrometers with high spectral resolution to find emission peaks that appear rather isolated in the spectrum, so overlap and contributions from side peaks are minimized. A good example is the work of Peng et al., who studied the thermal dependence of $^5D_0 \rightarrow ^7F_2$ europium luminescence in Y_2O_3 nanocrystals and determined that, under 488 nm excitation, the spectral width was almost constant up to 70 K, but for higher temperatures varied linearly as $0.078 \text{ cm}^{-1}/\text{K}$ [90].

Alternatively, fluorescence lifetime can also be considered, since it is also independent of most non-thermal effects on luminescence (particle concentration, illumination power, pH, viscosity...). Lifetimes can however be affected by luminescence quenchers in the nanoparticle environment, as they can trigger non-radiative energy-transfer processes if they are sufficiently close to the nanoparticle or even adsorbed to its surface. Since non-radiative energy transfer is a distance-dependent phenomenon, only lanthanide ions that are close enough to external molecules are prone to interact with them. Accordingly, this limitation on the accuracy of

lifetimes for thermometry becomes more relevant for smaller particles. Still, if the fluorophore lifetime is calibrated in the solvent to be used during the application, lifetime is a robust parameter to use in nanothermometry. For low lanthanide doping concentrations the experimental lifetime of an emitting energy state, τ , can be divided into two different contributions: a radiative one, τ_{rad} , associated to the emission of photons, and a non-radiative one, τ_{NR} , mainly associated to the relaxation of the energy state by exchanging energy with the phonons of the crystal lattice (vibrations) and/or to external molecules, as mentioned above:

$$\frac{1}{\tau} = \frac{1}{\tau_{rad}} + \frac{1}{\tau_{NR}} \quad (7)$$

While radiative lifetime shows a weak dependence on temperature, non-radiative lifetime becomes shorter at higher temperatures, as the density of phonons increases. For larger concentrations of lanthanides, energy transfer processes between lanthanide ions start contributing to the non-radiative term, making the lifetime shorter. Since energy transfer mechanisms can be also supported by phonons, they can add further complexity to the dependency of lifetimes with temperature [91]. We illustrate in **Figure 14A** the thermal dependence of the lifetime of several materials doped with fixed concentrations of lanthanide ions (and some transition metals). A thermal threshold is observed in most cases, which differentiates two different regimes. Below the threshold the lifetime is almost constant with temperature because vibrational transitions are unlikely, while above the threshold vibrational contributions become active and the lifetime decreases faster with temperature [92]. The temperature at which the threshold occurs depends mainly on the energy of lattice phonons (and thus on the crystal host), and on the energy separation between the emitting state and the lower lying state of the lanthanide, which is the separation that needs to be bridged by phonons to

obtain a non-radiative transition [10]. Lifetime can thus be used for thermometry, as long as the thermal range of interest is above the threshold.

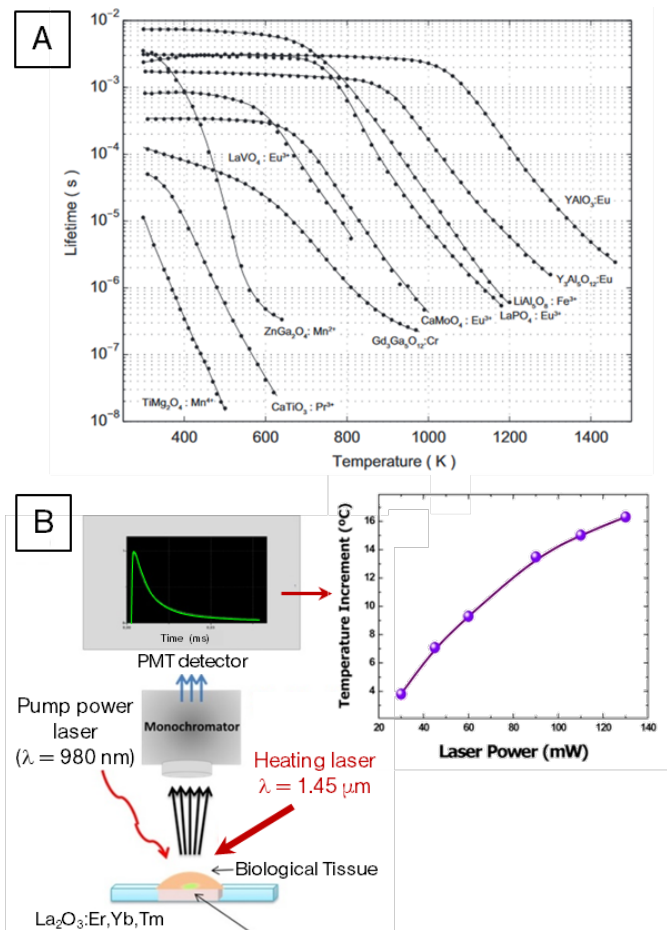


Figure 14. (A) Variation of lifetime with temperature for several lanthanide-doped materials (note that some materials are doped with transition metals instead). Reprinted from Ref. [92], with permission from Elsevier. (B) Scheme of the experimental set-up used to measure sub-tissue temperature by recording the lifetime of $\text{La}_2\text{O}_3:\text{Er}, \text{Yb}, \text{Tm}$ particles. The tissue was heated with a 980 nm laser, which is absorbed by water, generating a temperature increase that was plotted versus the laser power. Adapted from Ref. [93], with permission from Elsevier.

Despite its advantages, lifetime-based nanothermometry is not the most common technique based on lanthanides, probably because it requires a specific experimental set-up for time-resolved spectroscopy. Still, few interesting reports can be found, e.g. using the green emission of erbium ions excited at 980 nm in $\text{NaYF}_4:\text{Er}^{3+}, \text{Yb}^{3+}$ and $\text{NaY}_2\text{F}_5\text{O}:\text{Er}^{3+}, \text{Yb}^{3+}$ nanoparticles, to

measure the heat induced by laser illumination in *ex vivo* experiments using chicken breast. Normalized sensitivities of 0.5 %K⁻¹ and 1.5 %K⁻¹ were obtained, respectively, demonstrating the importance of the host in terms of sensitivity optimization [94]. A related experiment using La₂O₃:Er³⁺, Tm³⁺, Yb³⁺ instead (**Figure 14B**), yielded a sensitivity of 0.67 %K⁻¹ for the blue emission of thulium, excited through upconversion [93].

From the experimental point of view, the emission intensity is probably the simplest probe choice. The intensity of the emission bands of lanthanides decreases with temperature, mainly due to non-radiative transitions (**Figure 10B**), which are more likely when the energy gap gets shorter, until the lower lying state. Therefore, the intensity vs. temperature rate depends on the energy distance between both levels, and is thus different for each emission band. This could in principle be a major source of optical thermometers. However, as it happens with every other fluorophore, changes in emission intensity can be related to other causes than temperature, such as inhomogeneous particle distribution within the sample, fluctuations in illumination power or the presence of luminescence quenchers in the medium. To overcome these limitations, the availability of more than one emission band in the luminescent spectrum of lanthanide-doped materials largely facilitates the design of ratiometric intensity-based thermometers. In the case of organic dyes, the use of two different luminescent molecules as probe and reference involved problems related to careful control of spatial distribution, whilst in lanthanide-doped materials co-localization of the reference and the probe is guaranteed, as they come from the same particle. In principle, any two emission bands can be selected to construct the thermometer. However, from the experimental point of view, it is convenient that both emission wavelengths are close to each other. Furthermore, if we think of an application comprising an inhomogeneous medium, as often happens in biology where the solvent has a complex absorption spectrum, the wavelength

proximity between reference and probe becomes a requisite. Finally, it should be noted that for the intensity ratio to solve the problem of fluctuating excitation powers, both emission bands must depend equally on power, which is usually the case in standard luminescence experiments. This is however not necessarily the case for excitation mechanisms based on upconversion, where emission intensity depends on excitation power following a power law where the number in the exponent is defined by the upconversion path populating each energy state [95]. Accordingly, if a ratio is defined by two of these independent emissions, it must be considered that the link between intensity ratio and temperature might not be independent on the illumination power.

In certain lanthanide-doped materials however, all these limitations can be at least partially solved. This is when both emission bands are energetically close to each other, so their electronic populations are thermally linked, i.e. such that an electron from the lower state can get promoted to the upper state due to thermal energy. Both states must also be sufficiently separated to allow their spectral resolution. It has been reported that the optimal separation should be between 200 and 2000 cm^{-1} [96]. Under these conditions, thermal coupling results in an intensity ratio between emission bands, I_1/I_2 , following a Boltzmann distribution,

$$\frac{I_1}{I_2} = B \exp\left(-\frac{\Delta E}{k_B T}\right) \quad (8)$$

where ΔE is the energy gap between both levels and B is a constant that depends on the material and the optical set-up, and thus needs to be determined for each experiment [97] (alternatively, once ΔE is known, it is possible to calculate I_1/I_2 at room temperature instead of determining B , which results in a simpler experiment) [98]. Thermalized energy states can be found within the same emission band between Stark sublevels, as is the case for some Nd^{3+} -based thermometers

[99], or between two different emission bands, as in Er^{3+} thermometers, where the green emissions (**Figure 13B and 13C**) are thermally linked [97]. In this case, the thermal dependence is very stable as most parameters affecting the luminescence of the thermalized states do not affect the population balance between them. As a consequence, systems based on this effect have been applied to a variety of applications including intracellular thermometry [100], characterization of plasmonic heating [101, 102] or characterization of microelectronic circuits by incorporating an $\text{Er}^{3+}, \text{Yb}^{3+}$ -doped particle onto the tip of a cantilever to carry out scanning thermal imaging [103].

The thermal sensitivity of this technique largely depends on the lanthanide ions selected for the thermometer, but also on the inorganic host. For instance, in the case of $\text{Er}^{3+}, \text{Yb}^{3+}$ -doped materials it can range between 0.05 \%K^{-1} (in zirconian glass) and more than 1.4 \%K^{-1} (in LiNbO_3), demonstrating the importance of the selected crystal host [97].

We have discussed here the main ways in which lanthanide-doped nanoparticles can be used to measure temperature. It is worth emphasizing that nanoparticles can be designed to display luminescence in the UV and visible ranges, and can also be excited through upconversion. Alternatively, they can also be designed to emit in the near-IR, as well as to fit both absorption and emission bands within the transparency windows of biological tissues. Indeed, lanthanide-doped materials are, together with single-wall carbon nanotubes, the most advanced sensors working in the second and third biological transparency windows [104].

Up to this point, we have discussed materials comprising an inorganic host in which lanthanide ions are incorporated as dopants. However, this is not the only option, as they can be also incorporated into organic molecules. In this case, the organic-inorganic molecules can compose a

macromolecular crystalline complex through covalent interactions, known as metal-organic frameworks (MOFs). Most of the MOFs developed for thermometry are based on the emission ratio between europium and terbium [105], but several attempts have also been made with alternative sources of luminescence, such as excimer emission instead of Eu^{3+} [106], emission of the organic ligand instead of Eu^{3+} or Tb^{3+} [107], or the use of Dy^{3+} [108]. An extensive review on this precise subject was recently published, and provides detailed information on these options [109]. The thermometric technique is based on an intensity ratio, commonly between Eu^{3+} and Tb^{3+} emissions. Both ions are excited via illumination to the singlet state of the ligand (typically at wavelengths in the near-UV range), which transfers energy into both Eu^{3+} and Tb^{3+} . Alternatively, the triplet state of the ligand can be excited from the singlet state, and then it becomes the donor state in the energy transfer process populating Eu^{3+} and Tb^{3+} . In any case, both lanthanide ions follow the same excitation route, and thus their intensity ratio becomes a solid parameter, regardless of the excitation power. As the energy transfer from the ligand to the lanthanides is non-resonant, it requires the assistance of phonons, and thus it depends on temperature. Accordingly, the ratio between the emissions of Eu^{3+} ($^5\text{D}_0 \rightarrow ^7\text{F}_2$ transition, ~615 nm) and Tb^{3+} ($^5\text{D}_4 \rightarrow ^7\text{F}_5$ transition, ~540 nm) is also thermally dependent. The maximum relative sensitivity of the thermometers varies strongly depending on the exact composition of the MOF, and typically ranges between 0.1 \%K^{-1} and 10 \%K^{-1} [109, 110]. From the application point of view, these thermometers stand out due to the broad range of temperatures in which they have been demonstrated to perform. Indeed, there are few examples of compositions that present high sensitivities (between 1 \%K^{-1} and 10 \%K^{-1}) in the cryogenic range, and thus are proposed for applications dealing with them, as might be the case in aerospace industry or regarding superconducting magnets, to cite some [111-113].

5.4. Diamond nanoparticles

Among the nanomaterials most recently proposed for remote nanothermometry are diamond nanoparticles or nanodiamonds [17]. As major features, the inertness of nanodiamonds allows their use in harsh conditions; their thermal stability renders them useful within a wide thermal range (200 – 600 K); while their low toxicity facilitates their use as sensors in biological environments. The technique additionally offers high thermal sensitivity and resolution, but requires a more complex experimental set-up than those used for standard luminescence experiments, due to the high sensitivity of nanodiamonds to external magnetic fields. The nanoparticles used here are diamonds with a certain concentration of defects that act as color centers and modify the optical properties of the material. In particular, useful defects comprise negatively charged nitrogen vacancies (NV^-), i.e. substitutional nitrogen atoms adjacent to a carbon vacancy that has trapped an additional electron (**Figure 15B**). The centers can be excited to the first excited state, 3E , with green illumination, and they subsequently generate emission between 637 and 800 nm (**Figure 15A**, $^3E \rightarrow ^3A_2$ transition). The ground state of the defects is a triplet with $m_s = 0$ and $m_s = \pm 1$ split by spin-spin interactions (zero-field), while breaking the degeneracy of $m_s = \pm 1$ requires an external magnetic field. In the absence of such a field, the energetic separation between both m_s states depends on temperature due to thermally induced lattice strains. The thermometry technique is thus based on accurately determining the energetic separation, which can be done optically.

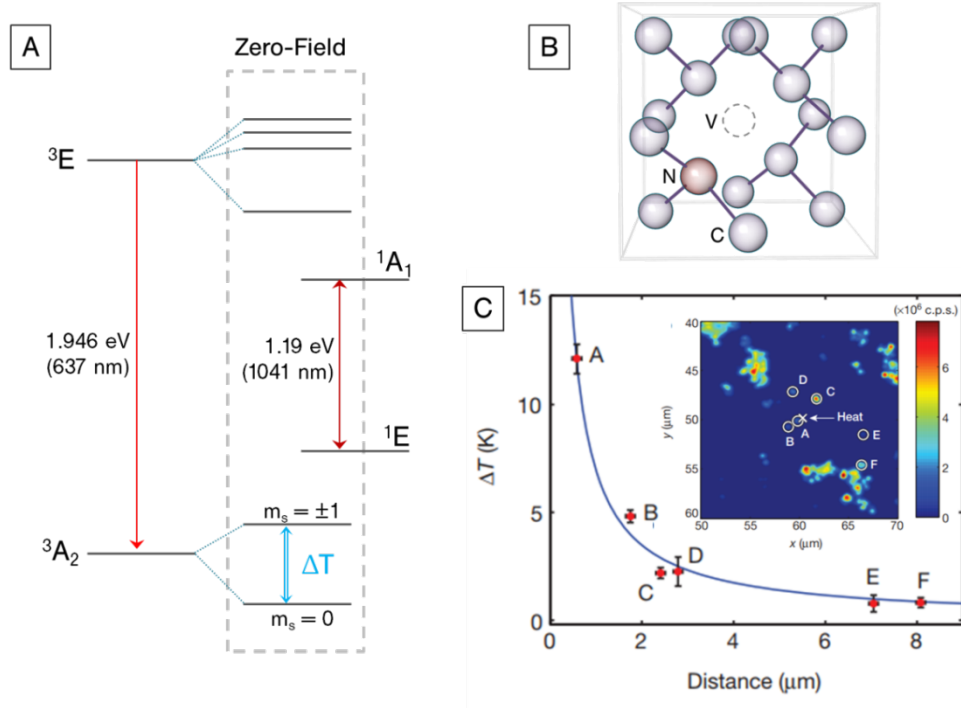


Figure 15. (A) Simplified energy diagram of NV^- defects in diamond, showing the zero-field splitting, which is responsible for degeneracy rupture of the ground state. The separation between both m_s states depends on temperature, although distortions can also be introduced by an external magnetic field. (B) Diamond lattice showing a NV^- defect with a substitutional nitrogen atom and a related vacant. (C) Plot of the temperature measured by nanodiamonds at different distances of a gold nanorod that behaves as source of heat. The inset shows the spatial location of each nanodiamond (letters) and the gold nanorod (labelled as “heat”). Reprinted by permission from Springer Nature, Ref [17]. Copyright 2013.

G. Kucsko et al. demonstrated the possibility of using nanodiamonds to measure the temperature gradient created by an excited gold nanorod. In order to do so, the high sensitivity of $m_s = \pm 1$ states toward magnetic fields makes it necessary to start by decoupling the defect from external unwanted fluctuating fields, which is done by recording the response of the defect to a sequence of microwave 2π echo pulses. To determine temperature, they then recorded a continuous-wave electron spin resonance (ESR) spectrum in which fluorescence was measured at four different microwave frequencies to improve the accuracy of the result. To demonstrate that the technique is valid in different environments, the experiment was done first on a spin-coated sample

containing both nanodiamonds and gold nanorods that behaved as local heaters under irradiation of their localized plasmon resonance, achieving a thermal resolution of ca. 0.05 K (**Figure 15C**). Thermal measurements were also demonstrated inside live cells, with equivalent results [17]. An alternative strategy proposed to measure temperature using NV⁻ defects in nanodiamonds exploited the temperature dependence of the optical Debye-Waller (incoherent neutron scattering) factor. This contribution generates a diffuse background in the optical signal that is used to define a ratio with the emission of the center, constituting an all-optical technique [114].

6. Latest progress towards applications, conclusions and perspective

No universal solution exists to answer all the needs of nanothermometry. However, the field is growing fast, providing numerous strategies that can be adapted to a wide variety of situations. From the experimental point of view, there is a need to develop protocols allowing for accurate temperature determination, either through scanning thermal microscopy, non-contact optical techniques, or through the use of fluorophores. In order to do so, it is essential to understand the mechanisms governing the behavior of the nano-thermometer, in particular to determine (and hopefully to control or at least avoid) all possible sources of error.

Although nanothermometry techniques are starting to be applied in real situations, their use is not extensive yet. They are in a stage in which their application requires careful testing to guarantee a fair thermal reading and to develop them towards standardization. This is a challenge partly due to a limited access to the required experimental set-ups in laboratories where samples are to be tested (often biological or engineering), but also because of the multidisciplinary character of the field. This need is evidenced, for instance, by the disagreement between experimental and theoretical approaches regarding intracellular thermal gradients.

The case of nanothermometry for biomedical applications is particularly challenging due to toxicity concerns and to the complexity of the environment where the thermometers should perform. Specifically, one of the major goals in this regard is related to the development of strategies that allow measuring precisely in the area of interest inside the patient's body. Since most thermometers are optical, an alternative is to use endoscopic tools with capacity to excite and collect light from the thermometers. However, in order to develop minimally invasive techniques, nanothermometers that are externally activated with light are preferred. Due to their composition, biological tissues present several ranges of low absorbance in the near-infrared, known as biological windows. When light is absorbed by tissues, it is largely transformed into heat and thus, operation at the wavelengths of lower absorption cross-section not only has the advantage of allowing the excitation light to get deeper inside the sample, but it is also the wavelengths range at which the environment gets less thermally modified. Additionally, scattering of light decreases as the wavelength increases, and thus, its effect is smaller in the near-infrared than in the visible or UV ranges. The wavelengths where these windows are located are 750-950 nm (first biological window), 1000-1450 nm (second biological window), and 1500-1700 nm (third biological window). Quite recently a fourth window was defined (2100 – 2300 nm) [115], and more may come, since research is currently active in the field.

The development of nanothermometers working within these ranges is one of the preferred routes, together with their implementation in actual biomedical applications, especially *in vivo* [104, 116, 117]. In fact, given the latest advances in the field, it can be expected that thermometry can go beyond the expected control of therapeutic techniques and even become a diagnostic tool. Among the examples of techniques implemented *in vivo*, there are some good examples that can illustrate this point. This is the case of the above mentioned (see section 5.2)

near-infrared emitting quantum dots (PbS/CdS/ZnS), which have been proposed to detect ischemia through thermometry measurements [78]. More specifically, this involves the determination of the thermal relaxation of tissues, which is different in healthy and affected areas. Within the same research group, quantum dots (PbS) emitting within the third biological window have been proposed for cardiovascular imaging, combining fluorescence with optical coherence tomography. In this case, thermometry is not demonstrated, but this example clearly shows the strong potential of near-infrared emitting nanoparticles in the biomedical field, and supports the idea that they can be used as multimodal probes [118]. However, these examples exploit the thermometric abilities of quantum dots, in which sensitive thermometry is best measured through an intensity-based technique. As intensity is affected by a variety of side-effects different to temperature, this technique only allows for the measurement of transient thermal changes, and not for the measurement of absolute temperatures. The category of materials working within the near-infrared range that can be used for the determination of absolute temperatures presently comprises lanthanide-doped nanoparticles. Unfortunately, in this case the sensitivity and the signal intensity are often not as high as in the case of quantum dots, and thus they are not a perfect option either. Accordingly, we propose that there is still a need for developing better near-infrared nanothermometers, to be used in biomedical applications. The solution may come from engineered lanthanide-doped nanoparticles with improved intensity and sensitivity. It is possible, for example, to increase the signal intensity by preparing core/shell structures [119], or by incorporating them into hybrid structures that contain antennae for the excitation, or plasmonic nanoparticles that can trigger the luminescent enhancement [101]. Regarding quantum dots, hybrid structures may also be a solution, in this case to implement a ratiometric technique through addition of a second fluorophore [120]. Most of these options are

currently under study, but have not been tested in actual applications yet, so their actual limitations are not obvious in all cases. In this regard, it is worth mentioning a recent piece of work which defined a ratiometric technique based on the luminescence of zinc gallogermanate nanoparticles doped with Cr^{3+} , whose performance was tested *in vivo* [121]. Whereas the emission was in this case within the first biological window (~ 700 nm), the excitation wavelength was in the UV. However, given the ultralong decay time of the luminescence, the authors demonstrated that it is possible to first excite the particles, then inject them into mice, and finally monitor the luminescence during more than three hours. This example illustrates that, besides the main avenues described above (quantum dots and lanthanide-doped materials), new options can still emerge as competitive alternatives.

A different route that nanothermometry should follow regarding biomedical applications is the combination of heating nanoparticles with nanothermometers, which would represent a relevant step forward in controlling and understanding hyperthermia treatments. Again, as a biomedical application, the proposed technique should operate in the near-infrared spectral range. Few attempts have been demonstrated toward this goal. Some of the thermometric particles described in this manuscript, can not only emit an optical signal with thermally dependent characteristics, but also partially release the absorbed energy into the environment in the form of heat, and can be specifically optimized to enhance this functionality. A key example is the case of neodymium-doped nanoparticles that in some hosts and above a certain doping range can present both functionalities [122-126]. This is naturally not the only option, as such heating/thermometric behavior has been also observed in PbS/CdS/ZnS quantum dots [127], and even demonstrated *in vivo*.

The use of a single material combining heating and thermal sensing ability benefits from the simplicity and robustness of the multifunctional probe. However, in such cases, the heating efficiency is not as high as that reached with different photothermal probes, such as magnetic or plasmonic nanoparticles. For this reason, several studies involved the preparation of hybrid structures that are optimized from both the heating and thermometry points of view. One of the best examples of the use of magnetic nanoparticles is the work of Piñol et al., who prepared nanostructures with a maghemite core decorated with Eu,Tb-organometallic structures on the surface [128], constituting a single structure comprising both functionalities. In this case, the core was magnetically excited to produce heat and created a temperature increase that was monitored precisely at the surface, using the thermometric emission of the Eu,Tb complex in the visible range.

Additional efforts have been devoted to the use of plasmonic rather than magnetic heating, because in such cases, both the thermometer and the heater can be optically excited and no magnetic field is required. The first examples were based on simply mixing both types of particles, allowing the measurement of the heating efficiency of the plasmonic structures [102], or monitoring subtissue plasmonic heating (phantom tissue was used in this case) [129]. This strategy demonstrated the importance and feasibility of monitoring temperature *in situ*, but lacks the ensured co-localization of both types of particles, since they are not linked in any way. To solve that issue, an attempt has been made to combine gold nanorods with Er,Yb-doped rods through ionic interactions. This work constitutes a good example, including *in vitro* tests of the usefulness of these hybrid structures [130]. However, due to the inhomogeneity of the sample and, in particular, to the fact that the thermometer works in the visible range, moving forward toward *in vivo* applications still requires a significant optimization effort. A recent strategy based

on gold nanorods coated with an Er,Yb-doped layer provides a step forward, regarding homogeneity and robustness, therefore representing an important contribution, but does not yet fulfill the near-infrared requirement [131]. As an alternative, another recent and innovative approach proposed the addition of thermometric properties to gold nanorods, by modifying their surface with a mechanoresponsive polymer (pNIPAAm) [132]. Thermometry in this case was based on the sensitivity of the plasmon resonance to the particle environment, therefore changing when the polymer was stretched or collapsed. This approach has however the drawback of a complex experimental set-up which is more difficult to export to different laboratories; however, it fully works within the biological windows, which is an important asset for the targeted applications. Still, in our opinion, there is a long way to go until we can obtain heating/thermometric nanostructures, in particular regarding their optimization in the biological windows and simplicity of use, with the ultimate goal of testing them *in vivo*.

Acknowledgements

M. Q. acknowledges financial support from the European Commission under the Marie Skłodowska-Curie program (H2020-MSCA-IF-2014_659021 - PHELLINI). L. M. L.-M. acknowledges funding from the Spanish MINECO (Grant # MAT2017-86659-R).

References

- [1] G. Jochen, M. Michel, G. Mahler, Observability of Extensive Variables, Quantum Thermodynamics, Springer, Berlin, Heidelberg 2009.
- [2] M. Kliesch, C. Gogolin, M. Kastoryano, A. Riera, J. Eisert, Phys. Rev. X, 4 (2014) 031019.
- [3] M. Hartmann, Contemp. Phys., 47 (2006) 89-102.
- [4] M. Hartmann, G. Mahler, O. Hess, Phys. Rev. Lett., 93 (2004) 080402.
- [5] M. Hartmann, Minimal length scales for the existence of local temperature, in: L. Carlos, F. Palacio (Eds.) Thermometry at the Nanoscale, Royal Society of Chemistry, Cambridge, UK, 2016.

- [6] P.R.N. Childs, Nanoscale thermometry and temperature measurement, in: L. Carlos, F. Palacio (Eds.) *Thermometry at the Nanoscale*, Royal Society of Chemistry, Cambridge, UK, 2016.
- [7] D. Jaque, F. Vetrone, *Nanoscale*, 4 (2012) 4301-4326.
- [8] C.D. Brites, P.P. Lima, N.J. Silva, A. Millán, V.S. Amaral, F. Palacio, L.D. Carlos, *Nanoscale*, 4 (2012) 4799-4828.
- [9] G. Vancoillie, Q. Zhang, R. Hoogenboom, *Polymeric Temperature Sensors*, in: L.D. Carlos, F. Palacio (Eds.) *Thermometry at the Nanoscale*, Royal Society of Chemistry, Cambridge, UK, 2016, pp. 190 - 236.
- [10] M.D. Dramicanin, *Methods Appl. Fluores.*, 4 (2016) 042001.
- [11] X.-D. Wang, O.S. Wolfbeis, R.J. Meier, *Chem. Soc. Rev.*, 42 (2013) 7834-7859.
- [12] T. Bai, N. Gu, *Small*, 12 (2016) 4590-4610.
- [13] S. Uchiyama, C. Gota, T. Tsuji, N. Inada, *Chem. Commun.*, 53 (2017) 10976-10992.
- [14] C. Wang, R. Xu, W. Tian, X. Jiang, Z. Cui, M. Wang, H. Sun, K. Fang, N. Gu, *Cell Res.*, 21 (2011) 1517-1519.
- [15] M. Suzuki, V. Tseeb, K. Oyama, S. Ishiwata, *Biophys. J.*, 92 (2007) L46-L48.
- [16] K. Okabe, N. Inada, C. Gota, Y. Harada, T. Funatsu, S. Uchiyama, *Nat. Commun.*, 3 (2012) 705.
- [17] G. Kucsko, P.C. Maurer, N.Y. Yao, M. Kubo, H.J. Noh, P.K. Lo, H. Park, M.D. Lukin, *Nature*, 500 (2013) 54-58.
- [18] J.-M. Yang, H. Yang, L. Lin, *ACS Nano*, 5 (2011) 5067-5071.
- [19] C. Gota, K. Okabe, T. Funatsu, Y. Harada, S. Uchiyama, *J. Am. Chem. Soc.*, 131 (2009) 2766-2767.
- [20] G. Baffou, H. Rigneault, D. Marguet, L. Jullien, *Nat. Methods*, 11 (2014) 899 - 901.
- [21] S. Kiyonaka, R. Sakaguchi, I. Hamachi, T. Morii, T. Yoshizaki, Y. Mori, *Nat. Methods*, 12 (2015) 801-802.
- [22] M. Suzuki, V. Zeeb, S. Arai, K. Oyama, S.i. Ishiwata, *Nat. Methods*, 12 (2015) 802-803.
- [23] G. Baffou, H. Rigneault, D. Marguet, L. Jullien, *Nat. Methods*, 12 (2015) 803-803.
- [24] B. Pandiripalli, Department of Industrial and Manufacturing Engineering, Wichita State University, Wichita, 2010, pp. 96.
- [25] C. McAlinden, J. Khadka, K. Pesudovs, *J. Cataract. Refr. Surg.*, 41 (2015) 2598-2604.
- [26] K. Kim, J. Chung, G. Hwang, O. Kwon, J.S. Lee, *ACS Nano*, 5 (2011) 8700 - 8709.
- [27] S. Gomès, A. Assy, P.-O. Chapuis, *Phys. Stat. Solidi A*, 212 (2015) 477-494.
- [28] O. Nakabeppu, M. Chandrachud, Y. Wu, J. Lai, A. Majumdar, *Appl. Phys. Lett.*, 66 (1995) 694 - 696.
- [29] R. Heiderhoff, A. Makris, T. Riedl, *Mater. Sci. Semicond. Process.*, 43 (2016) 163-176.
- [30] X. Xie, K.L. Grosse, J. Song, C. Lu, S. Dunham, F. Du, A.E. Islam, Y. Li, Y. Zhang, E. Pop, Y. Huang, W.P. King, J.A. Rogers, *ACS Nano*, 6 (2012) 10267-10275.

- [31] F. Yang, G. Li, J. Yang, Z. Wang, D. Han, F. Zheng, S. Xu, *Sci. Rep.*, 7 (2017) 1721.
- [32] Y. Gao, Y. Bando, *Nature*, 415 (2002) 599-599.
- [33] G. Baffou, P. Bon, J. Savatier, J. Polleux, M. Zhu, M. Merlin, H. Rigneault, S. Monneret, *ACS Nano*, 6 (2012) 2452 - 2458.
- [34] G. Baffou, J. Polleux, H. Rigneault, S. Monneret, *J. Phys. Chem. C*, 118 (2014) 4890 - 4898.
- [35] P. Bon, N. Bleaid, D. Lagrange, C. Bergaud, H. Rigneault, S. Monneret, G. Baffou, *Appl. Phys. Lett.*, 102 (2013) 244103.
- [36] S. Choi, E.R. Heller, D. Dorsey, R. Vetry, S. Graham, *IEEE Trans. Electr. Devices*, 60 (2013) 1898-1904.
- [37] S.D. McGrane, D.S. Moore, P.M. Goodwin, D.M. Dattelbaum, *Appl. Spectrosc.*, 68 (2014) 1279-1288.
- [38] M. Freitag, M. Steiner, Y. Martin, V. Perebeinos, Z. Chen, J.C. Tsang, P. Avouris, *Nano Lett.*, 9 (2009) 1883-1888.
- [39] X. Xie, D.G. Cahill, *Appl. Phys. Lett.*, 109 (2016) 183104.
- [40] K. Soo Ho, N. Jermim, J. Min Ku, K. Ki Woong, P.L. Luke, W. Seong Ihl, *J. Micromech. Microeng.*, 16 (2006) 526-530.
- [41] S. Senapati, K.K. Nanda, *ACS Appl. Mater. Interfaces*, 7 (2015) 23481-23488.
- [42] J. Lou, T.M. Finegan, P. Mohsen, T.A. Hatton, P.E. Laibinis, *Rev. Anal. Chem.*, 18 (1999) 235 - 284.
- [43] D. Lee, O. Bolton, B.C. Kim, J.H. Youk, S. Takayama, J. Kim, *J. Am. Chem. Soc.*, 135 (2013) 6325-6329.
- [44] D. Ross, M. Gaitan, L.E. Locascio, *Anal. Chem.*, 73 (2001) 4117-4123.
- [45] W.M. Abed, A.F. Domingues, R.J. Poole, D.J.C. Dennis, *Int. J. Therm. Sci.*, 121 (2017) 249-265.
- [46] Y.-W. Li, F.-G. Bian, J. Wang, *Nucl. Sci. Tech.*, 27 (2016) 92.
- [47] J. Marschewski, R. Brechbühler, S. Jung, P. Ruch, B. Michel, D. Poulikakos, *Int. J. Heat Mass Transfer*, 95 (2016) 755-764.
- [48] C. Paviolo, A. Clayton, S. McArthur, P. Stoddart, *J. Microsc.*, 250 (2013) 179 - 188.
- [49] J. Sakakibara, R.J. Adrian, *Exp. Fluids*, 26 (1999) 7-15.
- [50] C.E. Estrada-Pérez, Y.A. Hassan, S. Tan, *Rev. Sci. Instrum.*, 82 (2011) 074901.
- [51] J.A. Sutton, B.T. Fisher, J.W. Fleming, *Exp. Fluids*, 45 (2008) 869-881.
- [52] S. Arai, Ferdinandus, S. Takeoka, S.i. Ishiwata, H. Sato, M. Suzuki, *Analyst*, 140 (2015) 7534-7539.
- [53] Ferdinandus, S. Arai, S. Takeoka, S.i. Ishiwata, M. Suzuki, H. Sato, *ACS Sensors*, 1 (2016) 1222-1227.

- [54] T. Miyagawa, T. Fujie, Ferdinandus, T.T. Vo Doan, H. Sato, S. Takeoka, *ACS Appl. Mater. Interfaces*, 8 (2016) 33377-33385.
- [55] G.A. Baker, S.N. Baker, T.M. McCleskey, *Chem. Commun.*, (2003) 2932-2933.
- [56] M.T. Albelda, E. García-España, L. Gil, J.C. Lima, C. Lodeiro, J. Seixas de Melo, M.J. Melo, A.J. Parola, F. Pina, C. Soriano, *J. Phys. Chem. B*, 107 (2003) 6573-6578.
- [57] J. Feng, K. Tian, D. Hu, S. Wang, S. Li, Y. Zeng, Y. Li, G. Yang, *Angew. Chem. Int. Ed.*, 50 (2011) 8072 - 8076.
- [58] J. Feng, L. Xiong, S. Wang, S. Li, Y. Li, G. Yang, *Adv. Funct. Mater.*, 23 (2013) 340-345.
- [59] X. Liu, S. Li, J. Feng, Y. Li, G. Yang, *Chem. Commun.*, 50 (2014) 2778-2780.
- [60] H.D. Duong, J.I. Rhee, *Sens. Act., B*, 124 (2007) 18-23.
- [61] A. Pucci, F. Signori, R. Bizzarri, S. Bronco, G. Ruggeri, F. Ciardelli, *J. Mater. Chem.*, 20 (2010) 5843-5852.
- [62] Y. Wu, J. Liu, J. Ma, Y. Liu, Y. Wang, D. Wu, *ACS Appl. Mater. Interfaces*, 8 (2016) 14396-14405.
- [63] C. Pietsch, R. Hoogenboom, U.S. Schubert, *Polym. Chem.*, 1 (2010) 1005-1008.
- [64] K. Van Durme, G. Van Assche, B. Van Mele, *Macromolecules*, 37 (2004) 9596-9605.
- [65] B.H. Lessard, E.J.Y. Ling, M. Marić, *Macromolecules*, 45 (2012) 1879-1891.
- [66] A. Kawski, *Crit. Rev. Anal. Chem.*, 23 (1993) 459-529.
- [67] G. Baffou, M.P. Kreuzer, F. Kulzer, R. Quidant, *Opt. Express*, 17 (2009) 3291-3298.
- [68] H. Zhou, M. Sharma, O. Berezin, D. Zuckerman, M.Y. Berezin, *ChemPhysChem*, 17 (2016) 27-36.
- [69] J.S. Donner, S.A. Thompson, M.P. Kreuzer, G. Baffou, R. Quidant, *Nano Lett.*, 12 (2012) 2107-2111.
- [70] J.S. Donner, S.A. Thompson, C. Alonso-Ortega, J. Morales, L.G. Rico, S.I.C.O. Santos, R. Quidant, *ACS Nano*, 7 (2013) 8666-8672.
- [71] G.D. Scholes, G. Rumbles, *Nat. Mater.*, 5 (2006) 683 - 696.
- [72] D. Jaque, J. García Solé, *Quantum Dot Fluorescence Thermometry*, in: L. Carlos, F. Palacio (Eds.) *Thermometry at the Nanoscale*, Royal Society of Chemistry, Cambridge, UK, 2016.
- [73] W. Russ Algar, K. Susumu, J.B. Delehanty, I.L. Medintz, *Anal. Chem.*, 83 (2011) 8826-8837.
- [74] E. Petryayeva, W. Russ Algar, I.L. Medintz, *Appl. Spectrosc.*, 67 (2013) 215-252.
- [75] K.M. Tsoi, Q. Dai, B.A. Alman, W.C.W. Chan, *Acc. Chem. Res.*, 46 (2013) 662-671.
- [76] E. Oh, R. Liu, A. Nel, K.B. Gemill, M. Bilal, Y. Cohen, I.L. Medintz, *Nat. Nanotechnol.*, 11 (2016) 479-486.
- [77] S.S. Laha, A.R. Naik, E.R. Kuhn, M. Alvarez, A. Sujkowski, R.J. Wessells, B.P. Jena, *Nano Lett.*, 17 (2017) 1262-1268.

- [78] E.C. Ximendes, U. Rocha, B. del Rosal, A. Vaquero, F. Sanz-Rodríguez, L. Monge, F. Ren, F. Vetrone, D. Ma, J. García-Solé, C. Jacinto, D. Jaque, N. Fernández, *Adv. Healthc. Mater.*, 6 (2017) 1601195.
- [79] P. Jing, J. Zheng, M. Ikezawa, X. Liu, S. Lv, X. Kong, J. Zhao, Y. Masumoto, *J. Phys. Chem. C*, 113 (2009) 13545-13550.
- [80] Y. Zhao, C. Riemersma, F. Pietra, R. Koole, C. de Mello Donega, A. Meijerink, *ACS Nano*, 6 (2012) 9058 - 9067.
- [81] G. Morello, M. De Giorgi, S. Kudera, L. Manna, R. Cingolani, M. Anni, *J. Phys. Chem. C*, 111 (2007) 5846-5849.
- [82] P. Haro-Gonzalez, L. Martinez-Maestro, I.R. Martin, J. García-Solé, D. Jaque, *Small*, 8 (2012) 2652-2658.
- [83] A. Olkhovets, R. Hsu, Lipovskii, F. Wise, *Phys. Rev. Lett.*, 81 (1998) 3539 - 3542.
- [84] M.L. Debasu, D. Ananias, I. Pastoriza-Santos, L.M. Liz-Marzán, J. Rocha, L.D. Carlos, *Adv. Mater.*, 25 (2013) 4868-4874.
- [85] L. Martínez Maestro, E. Martin Rodriguez, F. Sanz Rodriguez, M.C. Iglesias-de la Cruz, A. Juarranz, R. Naccache, F. Vetrone, D. Jaque, J.A. Capobianco, J. García Solé, *Nano Lett.*, 10 (2010) 5109-5115.
- [86] I. Villa, A. Vedda, I.X. Cantarelli, M. Pedroni, F. Piccinelli, M. Bettinelli, A. Speghini, M. Quintanilla, F. Vetrone, U. Rocha, C. Jacinto, E. Carrasco, F.S. Rodriguez, A. Juarranz, B. del Rosal, D.H. Ortgies, P.H. Gonzalez, J.G. Sole, D.J. Garcia, *Nano Res.*, 8 (2015) 649-665.
- [87] A. Freeman, R. Watson, *Phys. Rev.*, 127 (1962) 2058-2075.
- [88] B. Henderson, G.F. Imbusch, *Optical spectroscopy of inorganic solids*, Oxford University Press, Oxford, 1989.
- [89] G. Dieke, *Spectra and energy levels of rare-earth ions in crystals*, Wiley, New York, 1968.
- [90] H. Peng, H. Song, B. Chen, J. Wang, S. Lu, X. Kong, J. Zhang, *J. Chem. Phys.*, 118 (2003) 3277-3282.
- [91] R. Reisfeld, M. Eyal, *J. Phys. Colloq.*, 46 (1985) 349-355.
- [92] J. Brübach, C. Pflitsch, A. Dreizler, B. Atakan, *Prog. Energ. Combust.*, 39 (2013) 37-60.
- [93] A. Siaï, P. Haro-Gonzalez, K. Horchani-Naifer, M. Férid, *Sens. Act., B*, 234 (2016) 541-548.
- [94] O.A. Savchuk, P. Haro-Gonzalez, J.J. Carvajal, D. Jaque, J. Massons, M. Aguiló, F. Díaz, *Nanoscale*, 6 (2014) 9727 - 9733.
- [95] M. Pollnau, D.R. Gamelin, S.R. Lüthi, H.U. Güdel, *Phys. Rev. B*, 61 (2000) 3337-3346.
- [96] V.K. Rai, *Appl. Phys. B*, 88 (2007) 297-303.
- [97] M. Quintanilla, E. Cantelar, F. Cusso, M. Villegas, A.C. Caballero, *Appl. Phys. Express*, 4 (2011) 022601.

- [98] S. Balabhadra, M.L. Debasu, C.D.S. Brites, R.A.S. Ferreira, L.D. Carlos, *J. Phys. Chem. C*, 121 (2017) 13962-13968.
- [99] A. Benayas, B. del Rosal, A. Pérez-Delgado, K. Santacruz-Gómez, D. Jaque, G.A. Hirata, F. Vetrone, *Adv. Opt. Mater.*, 3 (2015) 687-694.
- [100] F. Vetrone, R. Naccache, A. Zamarron, A.J.d.l. Fuente, F. Sanz-Rodriguez, L.M. Maestro, E.M. Rodriguez, D. Jaque, J.G. Sole, J.A. Capobianco, *ACS Nano*, 4 (2010) 3245 - 3258.
- [101] S. Rohani, M. Quintanilla, S. Tuccio, F. de Angelis, E. Cantelar, A.O. Govorov, L. Razzari, F. Vetrone, *Adv. Opt. Mater.*, 3 (2015) 1606-1613.
- [102] L. M. Maestro, P. Haro-Gonzalez, A. Sanchez-Iglesias, L.M. Liz-Marzan, J. García Solé, D. Jaque, *Langmuir*, 30 (2014) 1650-1658.
- [103] L. Aigouy, G. Tessier, M. Mortier, B. Charlot, *Appl. Phys. Lett.*, 87 (2005) 184105.
- [104] E. Hemmer, A. Benayas, F. Legaré, F. Vetrone, *Nanoscale Horizons*, 1 (2016) 168.
- [105] A. Cadiou, C.D.S. Brites, P.M.F.J. Costa, R.A.S. Ferreira, J. Rocha, L.D. Carlos, *ACS Nano*, 7 (2013) 7213-7218.
- [106] D. Ananias, A.D.G. Firmino, R.F. Mendes, F.A.A. Paz, M. Nolasco, L.D. Carlos, J. Rocha, *Chem. Mater.*, 29 (2017) 9547-9554.
- [107] R.F. D'Vries, S. Alvarez-Garcia, N. Snejko, L.E. Bausa, E. Gutierrez-Puebla, A. de Andres, M.A. Monge, *J. Mater. Chem. C*, 1 (2013) 6316-6324.
- [108] T. Xia, Y. Cui, Y. Yang, G. Qian, *J. Mater. Chem. C*, 5 (2017) 5044-5047.
- [109] J. Rocha, C.D.S. Brites, L.D. Carlos, *Chem. Eur. J.*, 22 (2016) 14782-14795.
- [110] A.M. Kaczmarek, Y.-Y. Liu, C. Wang, B. Laforce, L. Vincze, P. Van Der Voort, R. Van Deun, *Dalton Trans.*, 46 (2017) 12717-12723.
- [111] D. Ananias, C.D.S. Brites, L.D. Carlos, J. Rocha, *Eur. J. Inorg. Chem.*, 2016 (2016) 1967-1971.
- [112] I. N'Dala-Louika, D. Ananias, C. Latouche, R. Dessapt, L.D. Carlos, H. Serier-Brault, *J. Mater. Chem. C*, 5 (2017) 10933-10937.
- [113] X. Liu, S. Akerboom, M.d. Jong, I. Mutikainen, S. Tanase, A. Meijerink, E. Bouwman, *Inorg. Chem.*, 54 (2015) 11323-11329.
- [114] T. Plakhotnik, M.W. Doherty, J.H. Cole, R. Chapman, N.B. Manson, *Nano Lett.*, 14 (2014) 4989-4996.
- [115] L. Shi, L.A. Sordillo, A. Rodríguez-Contreras, R. Alfano, *J. Biophotonics*, 9 (2016) 38-43.
- [116] B. del Rosal, E. Ximendes, U. Rocha, D. Jaque, *Adv. Opt. Mater.*, 5 (2017) 1600508.
- [117] E. Hemmer, P. Acosta-Mora, J. Mendez-Ramos, S. Fischer, *J. Mater. Chem. B*, 5 (2017) 4365-4392.

- [118] J. Hu, D.H. Ortgies, R. Aguliar Torres, N. Fernández, L. Porto, E. Martín Rodríguez, J. García Solé, D. Jaque, F. Alfonso, F. Rivero, *Adv. Funct. Mater.*, 27 (2017) 1703276.
- [119] A. Skripka, R. Marin, A. Benayas, P. Canton, E. Hemmer, F. Vetrone, *Phys. Chem. Chem. Phys.*, 19 (2017) 11825-11834.
- [120] E.N. Cerón, D.H. Ortgies, B. del Rosal, F. Ren, A. Benayas, F. Vetrone, D. Ma, F. Sanz-Rodríguez, J.G. Solé, D. Jaque, E.M. Rodríguez, *Adv. Mater.*, 27 (2015) 4781-4787.
- [121] J. Yang, Y.X. Liu, Y.Y. Zhao, Z. Gong, M. Zhang, S.T. Yan, H.C. Zhu, C.G. Liu, C.S. Xu, H. Zhang, *Chem. Mater.*, 29 (2017) 8119-8131.
- [122] L. Marciniak, A. Pilch, S. Arabasz, D. Jin, A. Bednarkiewicz, *Nanoscale*, 9 (2017) 8288-8297.
- [123] A. Bednarkiewicz, D. Wawrzynczyk, M. Nyk, W. Strek, *Appl. Phys. B*, 103 (2011) 847-852.
- [124] H. Suo, X. Zhao, Z. Zhang, C. Guo, *ACS Appl. Mater. Interfaces*, 9 (2017) 43438-43448.
- [125] E. Carrasco, B. del Rosal, F. Sanz-Rodríguez, Á.J. de la Fuente, P.H. Gonzalez, U. Rocha, K.U. Kumar, C. Jacinto, J.G. Solé, D. Jaque, *Adv. Funct. Mater.*, 25 (2015) 615-626.
- [126] U. Rocha, K.U. Kumar, C. Jacinto, J. Ramiro, A.J. Caamaño, J.G. Solé, D. Jaque, *Appl. Phys. Lett.*, 104 (2014) 053703.
- [127] B. del Rosal, E. Carrasco, F. Ren, A. Benayas, F. Vetrone, F. Sanz-Rodríguez, D. Ma, Á. Juarranz, D. Jaque, *Adv. Funct. Mater.*, 26 (2016) 6060-6068.
- [128] R. Piñol, C.D.S. Brites, R. Bustamante, A. Martínez, N.J.O. Silva, J.L. Murillo, R. Cases, J. Carrey, C. Estepa, C. Sosa, F. Palacio, L.D. Carlos, A. Millán, *ACS Nano*, 9 (2015) 3134-3142.
- [129] U. Rocha, C.J. da Silva, W. Ferreira Silva, I. Guedes, A. Benayas, L. Martínez Maestro, M. Acosta Elias, E. Bovero, F.C.J.M. Van Veggel, J.A. García Solé, D. Jaque, *ACS Nano*, 7 (2013) 1188-1199.
- [130] M.L. Debasu, C.D.S. Brites, S. Balabhadra, H. Oliveira, J. Rocha, L.D. Carlos, *ChemNanoMat*, 2 (2016) 520-527.
- [131] Y. Huang, A. Skripka, L. Labrador-Paez, F. Sanz-Rodríguez, P. Haro-Gonzalez, D. Jaque, F. Rosei, F. Vetrone, *Nanoscale*, 10 (2018) 791-799.
- [132] X. Chen, Q. Xia, Y. Cao, Q. Min, J. Zhang, Z. Chen, H.-Y. Chen, J.-J. Zhu, *Nat. Commun.*, 8 (2017) 1498.